ARTICLE

https://doi.org/10.1590/2317-4889202120210043

BJGEO Brazilian Journal of Geology

Resende lamprophyres: new petrological and structural interpretations for a regional Upper Cretaceous alkaline mafic dyke swarm

Bruno Neves Macedo[1]*, Rodrigo Peternel[1], Anderson Costa dos Santos[1,2], Marcela Perroti Simas[1]

Abstract

New petrographic, lithogeochemical and structural analyses were performed on the Upper Cretaceous lamprophyres emplaced in the Proterozoic basement rocks of the Resende sedimentary basin in SE Brazil. Field characteristics and petrographic data confirm their identification as alkaline lamprophyres. Geochemical variations were mainly controlled by fractional crystallization of clinopyroxene and olivine. Liquid immiscibility, rapid cooling and crustal assimilation may have occurred subordinately during the evolution of the Resende lamprophyres. Mantle and chondrite-normalized diagrams point to an enriched mantle as the lamprophyre's magma source. Th/Yb and Ta/Yb ratios confirm a within-plate enriched mantle source with residual carbonate and phlogopite/amphibole as suggested by LILE enrichment and the presence of carbonate and phlogopite/amphibole as primary phases. The predominance of an ENE-trend of the dykes is related to a prevalent NNW-SSW orientation of the minimum principal stress (σ_3) orientation in an extensional regime during the emplacement of the Resende lamprophyres' dyke swarm. Frequent offsets produced by local dilation direction are parallel to the NNW-oriented extension of the main segments. WNW to NW secondary sets are controlled by previous discontinuities that were favored as pathways for the highly volatile lamprophyre magma. An NNW-SSE distension related to the Resende lamprophyre dyke swarm emplacement is consistent with the early stages of evolution of the Resende basin and uplift of its basement during the Late Cretaceous to the Paleocene.

KEYWORDS: lamprophyre dykes; Resende, fractional crystallization; Upper Cretaceous magmatism.

INTRODUCTION

Lamprophyres are known as exotic rocks, usually represented by dark-grey melanocratic/holomelanocratic intrusive bodies at shallow-crustal zones. They occur more frequently as thin dykes, usually less than one meter wide, even though sills and thicker bodies do also exist (*e.g.* Ubide *et al.* 2012). Lamprophyre rocks are porphyritic, comprising coexisting phenocrysts of anhydrous and hydrous ferromagnesian minerals, the latter usually biotite (phlogopite) and/or amphibole, with variable amounts of opaque minerals and apatite (Rock 1991). Anhydrous mafic minerals are represented by clinopyroxene and olivine. The usual aphanitic groundmass is composed of the same early phases with added alkali-feldspar, plagioclase, feldspathoids, and/or glass. A better explanation regarding the physical and chemical characteristics of lamprophyres is found in Rock (1991). The classification of lamprophyres is still a matter of debate (Streckeisen and Le Maitre 1979, Le Bas and Streckeisen 1991, Woolley *et al.* 1996, Tappe *et al.* 2005) despite the IUGS recommendations (Le Maitre 2002). High concentrations of MgO, K_2O, Na_2O, CO_2, H_2O, Ni and Cr are common in lamprophyres, as well as light rare earth elements (LREE) and large-ion lithophile elements (LILE) enrichment as opposed to high-field strength elements (HFSE) depletion (Rock 1991, Le Maitre 2002).

Dyke swarms are known as an effective mechanism to drain magmas from the lithosphere and/or asthenosphere through lower crust to shallower portions of the upper crust. In consonance, lamprophyre dykes are important kinematic markers and can provide fundamental information on emplacement mechanisms. Moreover, dyke swarm trends will reflect tensor systems associated with regional paleostress (Anderson 1951, Pollard 1973, Delaney *et al.* 1986). In general, dyke walls represent the σ_1-σ_2 plane whereas σ_3 is perpendicular, marking the extension direction assuming no shear component (Zoback 1992, Fossen 2010). However, magma can intrude previous discontinuities and may not represent the main regional stress. Delaney *et al.* (1986) developed a few criteria based on the relationship between dykes and joints (both adjacent and regional) to define whether an intrusion sheet can be used

[1]Programa de Pós-Graduação em Geociências, Faculdade de Geologia, Universidade do Estado do Rio de Janeiro – Rio de Janeiro (RJ), Brazil. E-mail: bneves.m@gmail.com, rpeternel@gmail.com, andcostasantos@gmail.com, marcela_simas@yahoo.com.br

[2]Geobiotec, Departamento de Geociências, Universidade de Aveiro – Aveiro, Portugal.

Supplementary data

Supplementary data associated with this article can be found in the online version: Supplementary Table A1, Supplementary Table A2 and Suplementary Map.

*Corresponding author.

as kinematic indicators. In addition, the so-called Bussel's Method (Bussel 1989) is a recognized as a valid procedure to derive the main distension axis based on dilation directions of the segments and other structural elements. These methods can provide the real paleotensor's position and validate deformation models (*e.g.* Ferrari 2001, Martínez-Poza *et al.* 2014, Stephens *et al.* 2017).

Although lamprophyres represent mostly sheet intrusions, only a few works use lamprophyre dykes or dyke swarms to determine paleostress activity during the respective magmatic event (*e.g.* Delaney *et al.* 1986, Martínez-Poza *et al.* 2014). In Southeast Brazil, several Upper Cretaceous lamprophyre dykes have been studied to constrain complex structural analyzes that aim to reconstruct the tectono-magmatic history of the so-called South American Platform (*e.g.* Ferrari 2001, Guedes *et al.* 2005, Motoki *et al.* 2008, Tomba 2012, Ferroni *et al.* 2018). These lamprophyre dykes occur nearby felsic alkaline stocks (Thompson *et al.* 1998) being related with the predominantly Upper Cretaceous to Paleogene alkaline magmatism along the Poços de Caldas-Cabo Frio Alignment and the Northern Serra do Mar Alkaline Province (Almeida 1983, Riccomini *et al.* 2005).

Near the Resende Basin, lamprophyre dykes are known as few isolated occurrences with scarce integrated data (*e.g.* Riccomini 1989, Riccomini *et al.* 1991, Thompson *et al.* 1998, Guedes *et al.* 2005, Marins 2012, Ferroni *et al.* 2018) that represents a not fully understood magmatic event. In addition, due to other mentions of the presence of indistinguishable thin mafic dykes on this region (Penalva 1967, Almeida 1996, Genaro 2008), and the fact that it is common to misinterpret these dykes as diabases on the field (Rock 1991), we did an extensive search to find new lamprophyre dykes and analyze them. We also visited known outcrops to collect structural data and confirm measurements. This paper presents new petrographic, geochemical, and structural data on the lamprophyre dykes that occur nearby the Resende sedimentary basin and the Itatiaia Alkaline Massif (IAM) in SE Brazil. These new and other compiled data from previous works in the same area (Rock 1991) will be used to place these bodies in a tectonomagmatic context, developing a structural model that accurately reflects paleostress conditions, also grouping, if possible, the lamprophyre dykes to the same magmatic event.

REGIONAL GEOLOGY

Mesozoic-Cenozoic tectonics and magmatism

The Alkaline Provinces of the South American Platform (Fig. 1A), mainly those located in central-southeastern Brazil were formed in the context of lower crust structural reactivations during the Jurassic Wealdenian Reactivation before the opening of the South Atlantic Ocean (Almeida 1983). Such reactivation would have triggered widespread alkaline magmatism, which was controlled by paleostructures. Magma formed under the parameters of thermal anomalies ascended, and gave rise to plutonic and volcanic bodies, stocks, plugs and dykes during

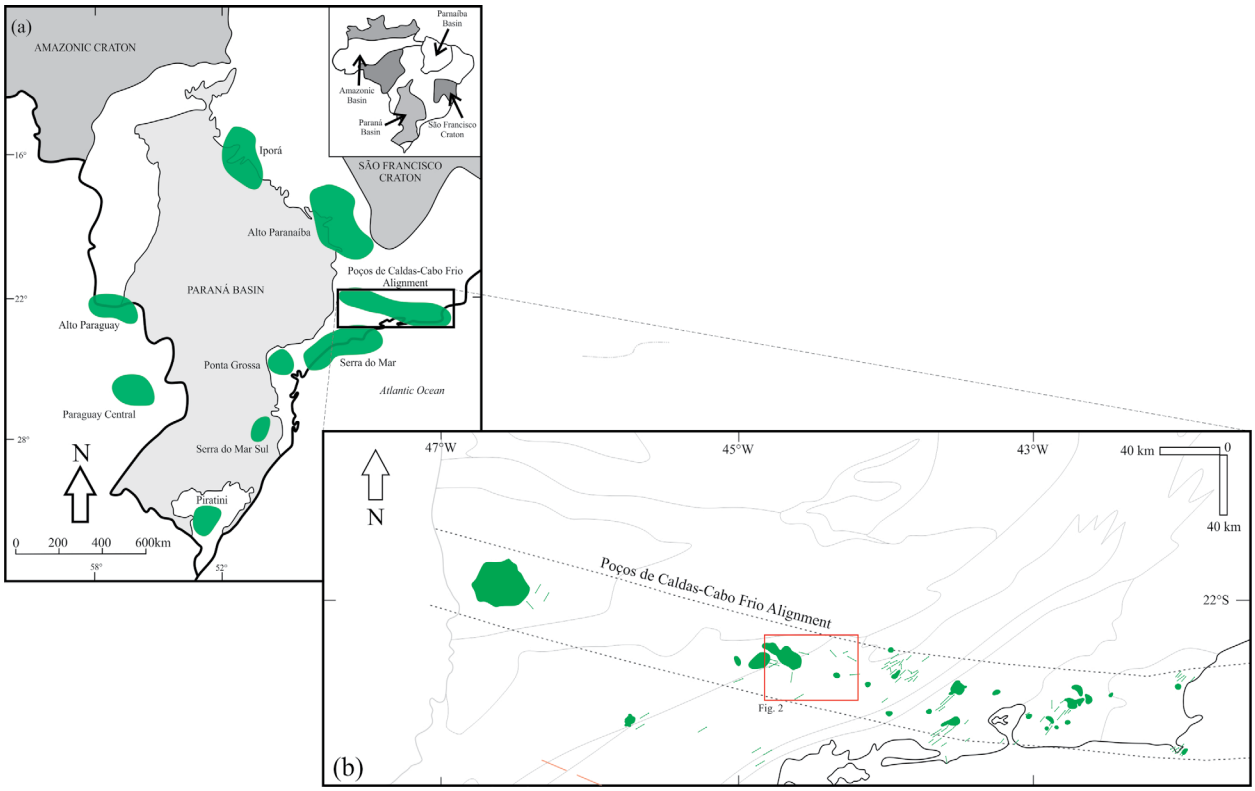

Figure 1. (A) Main alkaline provinces of Southeast Brazil (green areas) in the South American Platform. (B) Detail of the Poços de Caldas-Cabo Frio Alignment (within dotted lines) and its magmatic bodies, including mafic and felsic alkaline dykes. Compiled from Sadowski and Dias Neto (1981), Ulbrich and Gomes (1981), Almeida (1991), Araújo (1995), Valente (1997), Thompson *et al.* (1998), Ferrari (2001), Bennio *et al.* (2002), Guedes *et al.* (2005), Riccomini *et al.* (2005), Ulbrich *et al.* (2005), Valente *et al.* (2005), Motoki *et al.* (2007), Mota (2012), Azzone *et al.* (2018), Ventura and Valente (2017), Rosa (2017), and Ferroni *et al.* (2018). The Proterozoic basement contacts (grey lines) from Heilbron *et al.* (2000).

the Lower Cretaceous until, at least, the Paleogene. According to Riccomini *et al.* (2005), previous structures, such as different tectono-stratigraphic Proterozoic terrain boundaries and shear zones, played a fundamental role on the emplacement of alkaline igneous rocks. In addition, extending or occurring faults located at the edges of sedimentary basins and rifts also acted as controlling agents for the accommodation of some magmatic plutons (Zalán and Oliveira 2005).

Alkaline provinces are commonly found close to passive continental margins related to the formation of oceanic basins after continental breakup. The ascending alkaline magma succeeds the final phase of the tholeiitic magmatism characteristic of this environment during continental rifting (Fitton and Upton 1987). Predominantly, the provinces of the Central-Southeastern region (ca. 85-55 Ma) comprise extensive intrusive features (stocks and plugs) composed of evolved lithologies, mainly silica saturated or undersaturated plutons. These felsic alkaline rocks are time- and space-related with scarce, but not rare, basic or even ultrabasic lithologies predominantly restricted to lava flows, sills and mainly dykes (Morbidelli *et al.* 1995, Thompson *et al.* 1998, Gomes and Comin-Chiaramonti 2005). Alkaline mafic tabular intrusions are commonly classified as lamprophyres in several of these provinces (Garda *et al.* 1995, Valente 1997, Thompson *et al.* 1998, Gibson *et al.* 1999, Alves and Gomes 2001, Coutinho 2008, Azzone *et al.* 2009, Motoki *et al.* 2018).

The emplacement of the alkaline magma produced during the Wealdenian Reactivation was controlled by the numerous and well-determined Proterozoic crustal discontinuities (extending faults, suture zones and basin edges). Long-lived thermal anomalies located along the alkaline provinces would have been the cause of the production of the alkaline magma (Zalán and Oliveira 2005). However, some authors (Gibson *et al.* 1995, Thompson *et al.* 1998, Thomaz Filho and Rodrigues 1999, Santos 2013, 2016) suggest that the alkaline magmatism from the Iporá and Alto Paranaíba provinces (90 to 85 Ma), passing through the Poços de Caldas-Cabo Frio Magmatic Alignment (54 to 80 Ma) to the Vitória-Trindade Ridge (40 Ma to present day) (Fig. 1A) correspond to a nearly W-E mantle plume track. This hypothesis is based on the migration of the South American plate above a mantle plume in a WSW-ENE alignment (Herz 1977) and on the eastwards, apparent younger ages (Sonoki and Garda 1988, Thompson *et al.* 1998).

The Poços de Caldas-Cabo Frio magmatic alignment

The Poços de Caldas-Cabo Frio Magmatic Alignment (CFA; Sadowski and Dias Neto 1981, Almeida 1991, Riccomini *et al.* 2005) is an alkaline province with curved linear shape approximately 60 km wide and 1.200 km long (Fig. 1B). It encompasses several upper crust alkaline bodies, mostly intrusive on the crystalline basement assembled by Paleoproterozoic to Neoproterozoic metamorphic terrains (Heilbron *et al.* 2000, Schmitt *et al.* 2004, Trouw *et al.* 2013). Altogether, this alignment comprises more than 30 alkaline magmatic occurrences, including mainly felsic alkaline stocks such as Passa Quatro,

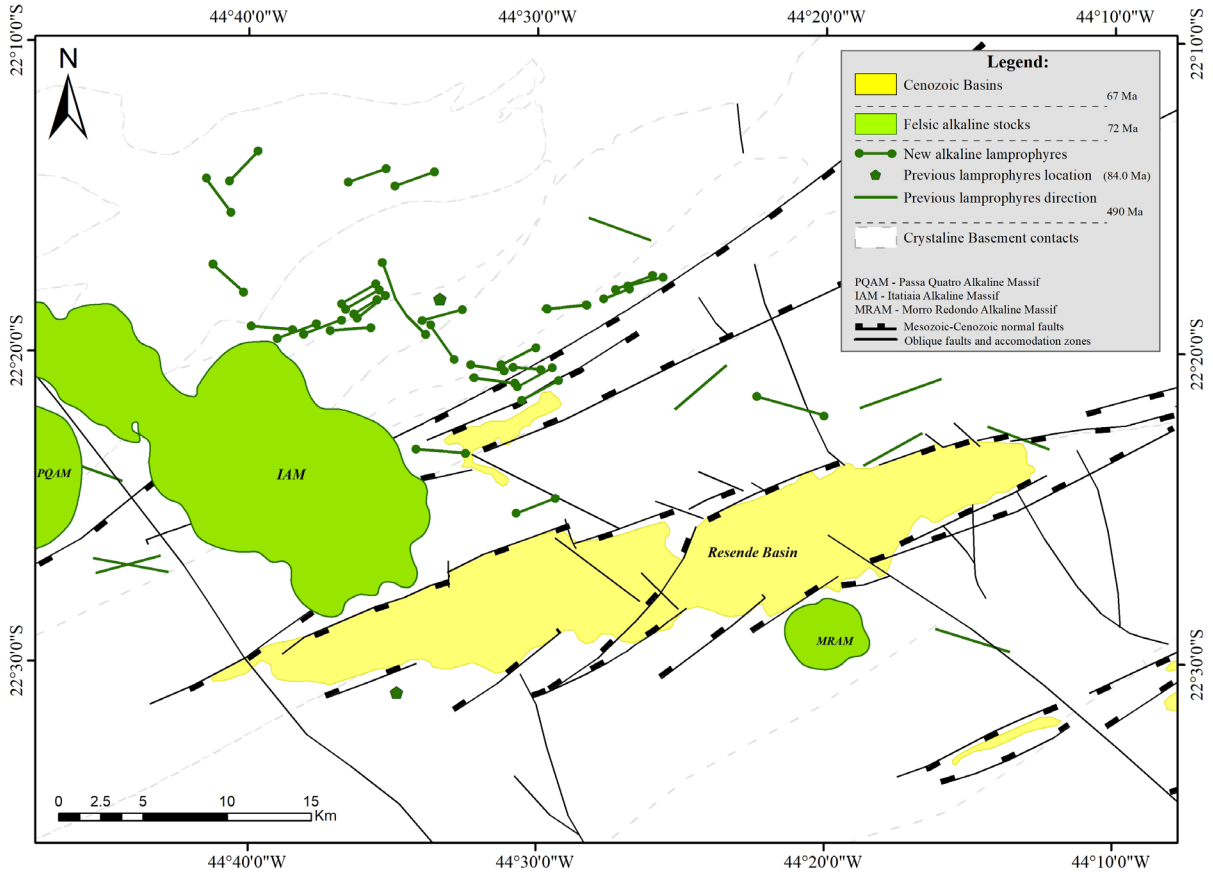

Figure 2. Geological sketch of the studied area with the focus on lamprophyre dykes. Sources: Riccomini (1989), Guedes *et al.* (2005), Zalán and Oliveira (2005), Rosa (2017), Ferroni *et al.* (2018), and Negrão *et al.* (2020). Basement contacts from Rio de Janeiro and Minas Gerais geological maps (Fonseca *et al.* 2014, Heilbron *et al.* 2016).

Itatiaia, Morro Redondo, Tomazes, Tinguá, Mendanha, Tanguá, Soarinho, Rio Bonito, Morro de São João and Cabo Frio. Most of these felsic alkaline massifs are subcircular in shape and predominantly composed of syenite and nepheline-syenite. Mafic and ultramafic rocks, and/or silica-oversaturated rocks, such as granites occur in a few of those alkaline massifs. Commonly, strongly silica-undersaturated and weakly silica-undersaturated mafic alkaline dykes, namely lamprophyres (or monchiquites and camptonites in general) and phonolites, as well as alkali-basalts and trachytes, respectively, are often associated with major intrusions (Brotzu *et al.* 2005), besides magmatic breccias (Motoki *et al.* 2010). Several authors have attributed the well-defined pattern of the Sr-Nd isotopic trend obtained for alkaline magmatic rocks of the South American Plate, including lamprophyre dykes, to an origin related with EM1 and HIMU components within an enriched heterogeneous mantle located in the subcontinental lithosphere (Gibson *et al.* 1995, Comin-Chiaramonti *et al.* 1997, Thompson *et al.* 1998).

The CFA possibly reflects a WNW-ESE crustal discontinuity (Almeida 1983, Brotzu *et al.* 2005). However, the main magmatic expressions would have been emplaced along NE- to NNE-trending subcrustal faults related to the Brasiliano Orogeny (ca. 590 Ma; and reactivated since the Cretaceous (Brotzu *et al.* 2005), explaining the NE-SW-trending stocks dyke swarms (Riccomini *et al.* 2005). Such configuration was possible for most alkaline massifs (from the Mendanha to the Cabo Frio stocks and dykes), due to the active far-field stress that started on the Upper Cretaceous on a sinistral transcurrent regime with the main compressive stress (σ_1) horizontally oriented along the NE-SW direction and the least compressive stress (σ_3) also horizontally oriented along the NW-SE direction (Ferrari 2001, Riccomini *et al.* 2005). The 80-50 Ma alkaline magmatism from the Mendanha Massif to the Cabo Frio Island Massif has been related with this deformational event (Ferrari 2001). Three extensional events along the NW-SE, NE-SW and EW directions occurred from the Eocene to the Holocene (Ferrari 2001), which explains the younger ages of the rocks within the Poços de Caldas-Cabo Frio Alignment Alkaline Province, supporting that the magmatism was controlled by reactivations of previous tensions and discontinuities (Riccomini *et al.* 2005). Part of the alkaline magmatism in the CFZ is coeval to brittle structures of the Continental Rift of Southeast Brazil (CRSB; Riccomini 1989). Most stocks are adjacent to Cenozoic basins and their emplacement were likely controlled by structures developed during the 134 to 114 Ma rift (Zalán and Oliveira 2005). During the rift phase of the South Atlantic opening, there was an intense reactivation of basement structures, predominantly trending NE-SW, which gave rise to the normal faults in the same direction, beyond transforming faults of NW-SE direction (Mohriak 2004). According to Zalán and Oliveira (2005), approximately 25 Ma after the rifting had ceased, the uplift of the basement occurred (89-65 Ma) coupled with the several alkaline magmatic pulses (*e.g.* dykes from Guedes *et al.* 2005 and Itatiaia stocks from Rosa 2017). Coeval to this pulse, in an extensional regime, basin edge faults (*e.g.* Santos Basin) represented the main weakness areas (Riccomini *et al.* 2005).

Several lamprophyres occur among minor dykes and sills mainly adjacent to alkaline felsic stocks and intrude the Paleoproterozoic metamorphic basement along different tectono-stratigraphic terrains (Fig. 1B; Ulbrich and Gomes 1981, Araújo 1995, Valente 1997, Thompson *et al.* 1998, Ferrari 2001, Guedes *et al.* 2005, Ulbrich *et al.* 2005, Valente *et al.* 2005, Motoki *et al.* 2007, Mota 2012, Ventura and Valente 2017, Ferroni *et al.* 2018). Along with alkaline felsic dykes, such as phonolites and trachytes, these sheet-like intrusions trend in predominantly NE-SW to ENE-WSW directions with minor NW- to WNW-oriented subsets. They represent shallow intrusions that mostly rise as earlier alkaline magmas (*e.g.* Cabo Frio lamprophyres; Motoki *et al.* 2008). Lamprophyre intrusions that occur exclusively on basement and cross-cut by felsic alkaline

Table 1. Main characteristics of the Resende lamprophyre dykes. Phenocryst: lowercase and uppercase; Groundmass: lowercase only. Abbreviations according to Whitney and Evans (2010): Clinopyroxene (cpx), olivine (ol), augite (aug), opaque minerals (opq), plagioclase (pl), analcite (anl), ocelli (ocl), carbonate (cb), biotite (bt), amphibole (amp), phlogopite (phl), k-feldspar (afs), kaersutite (krs), and magnetite (mgt). Representative sample identifications (ID) are indicated.

Authors	Sample ID	Lithology	Mineralogy	Age (Ma)	Method
Riccomini *et al.* (1991)	RE-06	Lamprophyre	Bt + Cpx ± Ol ± opq ± pl ± anl ± ocl	84 ± 3.0	$^{40}K/^{40}Ar$ - whole rock
Riccomini *et al.* (1991)	RE-07	Lamprophyre	Bt + Aug ± Ol ± opq ±pl ± anl ± ocl	-	-
Thompson *et al.* (1998)	94SOB90 (3)	Lamprophyre	Cpx + Ol + Mgt + Amp + Phl ± apt ± cpx ± amp ± bt ± opq ± afs ± glass (± spinel lherzolite xenoliths)	-	-
Guedes *et al.* (2005)	RE-II-39A	Monchiquite	Aug + Ol + afs ± aug ± opq ± krs ± opq ± glass	83.0 ± 1.0	$^{40}K/^{40}Ar$ - whole rock
Ramos *et al.* (2008)	RE-2	Lamprophyre	Bt + Cpx + pl ± opq	72.0 ± 0.4	$^{40}K/^{40}Ar$ - biotite
Marins (2012)	AGN-GM (6)	Monchiquite and camptonites	Aug + Ol ± Bt ± Krs ± opq ± apt ± cb	-	-
Ferroni *et al.* (2018)	ALC (9)	Alkaline lamprophyres	Phl + Cpx + phl + cpx ± opq ± ocl	-	-

dykes preclude these dykes as latter activities, despite the scarcity of clear relationship outcrops (*e.g.* Motoki *et al.* 2008). Some authors suggested that lamprophyres represent parental magmas to more evolved alkaline rocks found in some syenitic stocks by means of fractional crystallization (*e.g.* Brotzu *et al.* 1997, Thompson *et al.* 1998, Brotzu *et al.* 2005, Sichel *et al.* 2012) with little to no crustal assimilation (Enrich *et al.* 2005). In most cases of alkaline emplacement, this magmatism has a potassic to ultrapotassic affinity and variation in silica saturation (Brotzu *et al.* 1997).

GEOLOGICAL SETTING

Lamprophyres occurring nearby and inside the study area, hereafter called Resende lamprophyres, were described by other authors (Riccomini 1989, Riccomini *et al.* 1991, Thompson *et al.* 1998, Guedes *et al.* 2005, Ramos *et al.* 2008, Marins 2012, Ferroni *et al.* 2018) (Tab. 1). These lamprophyre dykes are intrusive in ENE- to NE-trending gneisses, amphibolites, and quartzites, as well as deformed granitoids, within an interference zone between two Upper Proterozoic collisional belts (Brasília and Ribeira belts) related with the Brasiliano Orogeny (Heilbron *et al.* 2004, Peternel *et al.* 2005, Trouw *et al.* 2013).

The Resende lamprophyres are thin (< 2 m thickness) sheet intrusions with diverse shapes. Part of them is aligned to the main basement foliation and brittle structures trending ENE-WSW, while others vary from WNW-ESE to NW-SE, following the regional fracturing direction (Fig. 2). The Resende lamprophyres are holomelanocratic to melanocratic, porphyritic to poikilitic rocks with typical pan-idiomorphic texture. Common phenocrysts are augite, pseudomorphic olivine, kaersutite, biotite and phlogopite, plus opaques and apatite in minor proportions. The phenocrysts are set in a groundmass that encompasses the same early phases in addition to feldspar, feldspathoid and/or glass, plus analcite, ocelli structures (carbonate plus analcime) and spinel lherzolite xenoliths. Secondary post-magmatic minerals are carbonate, chlorite, serpentine and iddingsite. The Resende lamprophyres are chemically classified as foidites and basanites/tephrites, with mostly potassic and rarely sodic types, bearing normative nepheline and olivine. They are considered products of the partial melting of the metasomatized, enriched subcontinental lithospheric mantle (*e.g.*, Brotzu *et al.* 2005, Enrich *et al.* 2005).

K-Ar whole-rock ages (84.0 ± 3 and 82.6 ± 1; Riccomini *et al.* 1991 and Guedes *et al.* 2005) were obtained for the Resende lamprophyres but K-Ar ages in biotite phenocrysts separated from a lamprophyre dyke in the northern portion of the study area yielded younger results (72 ± 0.4 Ma and 72.1 ± 0.4 Ma; Ramos *et al.* 2008). Thus, the Resende lamprophyre dykes may all be related with a prolonged magmatic event that took place in the Upper Cretaceous, Campanian age (Ferroni *et al.* 2018). Brotzu *et al.* (2005) and Enrich *et al.* 2005 proposed an evolutionary system with basanitic lamprophyres as parental magmas to more evolved felsic alkaline compositions in the nearby Itatiaia Alkaline Massif (IAM) by extensive fractional crystallization and no assimilation (Melluso *et al.* 2017). The same authors suggested a heterogeneously enriched subcontinental mantle source for the Resende lamprophyres, which is supported by previous studies (*e.g.* Brotzu *et al.* 1997, Valente 1997, Gibson *et al.* 1999, Marins 2012, Ferroni *et al.* 2018).

The IAM (Penalva 1967, Ribeiro Filho 1967) occurs in the western portion of the area and intrudes the Neoproterozoic gneisses of the Ribeira Belt (Fig. 2). It is a NW-SE-elongated pluton composed of felsic, alkaline silica under- to over-saturated igneous rocks (Brotzu *et al.* 1997, Brotzu *et al.* 2005, Enrich *et al.* 2005). Recently, alkaline mafic rocks were recognized and described in the IAM (Rosa and Ruberti 2018). New U/Pb ages point to magmatic activity between 71.3 and 67.5 Ma (Rosa 2017). Some authors (Brotzu *et al.* 1997, Thompson *et al.* 1998, Enrich *et al.* 2005) suggest that the differentiation processes in the IAM are related with possible basanite/tephritic precursor magmas evolving into the predominantly felsic, alkaline rocks of the IAM. The Passa Quatro (PQAM) and Morro Redondo alkaline massifs (MRAM) also occur in the study area (Fig. 2). The ENE-WSW-trending continental siliciclastic Resende sedimentary basin represents a tecto-no-sedimentary feature related with a regional Cenozoic rift system (Riccomini *et al.* 2004).

The structural framework of the study area displays a complex pattern and evolution. Tholeiitic dykes that intrude the ENE-WSW trending mylonitic basement are emplaced along two main directions (NNW-SSE and NNE-SSW), often thicker than 10 m (Guedes *et al.* 2005). The tholeiitic diabases are related to early stages of the Gondwana rifting that took place before the South Atlantic opening. They are roughly parallel to the NNW to NNE preferential regional fracturing directions, although NW-SE (Guedes *et al.* 2005) to WNW-ESE (Ferroni *et al.* 2018) trending intrusions can also be seen in the area. On the other hand, the mafic and felsic alkaline dykes, as well as the felsic alkaline stocks, trending orthogonal sets are related with the tectonic reactivations from the Upper Cretaceous to Paleogene (Guedes *et al.* 2005, Zalán and Oliveira 2005). The regional Cenozoic continental rifting is partially coeval to the Paleogene alkaline magmatism, forming sedimentary basins bounded by ENE-WSW normal faults and subordinated NW-SE transfer zones (Riccomini 1989, Zalán and Oliveira 2005). The evolution of the Resende Basin is attributed to an NNW-SSE extension during the Paleogene that caused ENE-trending normal faults with SSE-dipping grabens (Riccomini 1989, Riccomini *et al.* 2004, Negrão *et al.* 2015, Negrão *et al.* 2020). Riccomini *et al.* (2004) confirm an early NNW-SSE extension during the Paleogene prior to the sinistral transtensional regime along the Neogene.

ANALYTICAL METHODS

Petrography

Data for the current work was primarily collected in the field, where fifty samples were selected for thin section preparation in the Laboratório Geológico de Processamento de Amostras LGPA - UERJ, including a few metamorphic rocks from the

basement and Lower Cretaceous tholeiitic diabases. Thin sections of the less altered lamprophyre dykes were described under the ZEISS Axio Lab.A1 polarizing microscope at the LGPA. Photomicrographs were taken by a fitted camera and processed on the AxioVision 4.8.2 software. Modal analysis was done by counting 1,000 points per section and an average value was calculated whenever more than one thin section was described for a single lamprophyre dyke.

Lithogeochemistry

Six unaltered or less altered representative samples of the lamprophyres were selected for major and trace element analysis. Slabs were cleaned, dried, fragmented and pulverized at the LGPA (UERJ). The powdered samples were sent to the ALS Brazil Ltda laboratory (Vespasiano, Belo Horizonte, MG, Brazil). ICP-AES (inductively coupled plasma emission via atomic emission spectrometry) produced major element values. Trace element contents were done by ICP-MS (mass spectrometry). The loss on ignition (LOI) was measured at 1000°C using a WST-SEQ instrument and major and trace element data of 19 samples available in the literature were also compiled and used in this work for petrological interpretation. Geochemical data were not recalculated to a volatile-free basis as suggested by Woolley *et al.* (1996).

Structural geology

More than one hundred measurement data were obtained during field work, including tectonic foliation, fractures, veins, tholeiitic dykes and mainly lamprophyre dykes (dip direction and dip angle, and dilation planes). The structural characterization was divided in three steps:

- Geometrical analysis to determine the thickness and length of the dykes, dip direction and dip angle of all structures, and the relationship between then, according to the criteria in Delaney *et al.* (1986);
- Kinematic analysis to discriminate the movement features (dilation planes, fault planes, and slickensides/slickenlines). The consistent or inconsistent classification (Magee *et al.* 2019) and the Bussel's Method (Bussel 1989) on offset (non-faulted) lamprophyre dykes were applied, the latter based on dilation directions that represent planes constituted by offset edges and apparent dilation directions. Average dilation direction can be dictated by local or regional stress. Inconsistent stepping directions were not included on this analysis;
- Paleostress analysis, meaning geometrical and kinematic analysis integration and the application of straight dihedral method (Angelier 1991, 1994) was done with the use of the Wintensor 5.8.8 software (Delvaux and Sperner 2003).

RESULTS

Field aspects and petrography

Thirty-one new lamprophyre dykes were mapped in this work near to the Resende basin and the Itatiaia Alkaline Massif (Suppl. Map 1). All dykes crosscut exclusively the basement metamorphic rocks. Previously mapped bodies were visited and integrated to this research. A few up to 10 m thick diabase dykes are scattered in the study area and are distinguished from lamprophyres due to the presence of feldspar phenocrysts and alteration products (*e.g.* Rock 1991).

The lamprophyres of the Resende basin are thin dykes and sills with variable degrees of alteration that intruded high-grade metamorphic rocks (Fig. 3). The contacts between dykes and the country rocks are sharp, varying from straight to sinuous (Figs. 3A-3E). Segmentation and zigzag patterns are well exposed on sub-horizontal outcrops (Fig. 3A) whereas sub-vertical outcrops exhibit exclusively straight dykes. Chilled margins are common (Fig. 3D), and xenoliths are comprised of the regional gneisses. Alteration is depicted by a red to brown material embedding less altered biotite (phlogopite) and amphibole phenocrysts (Fig. 3E). The lamprophyres occur as ENE-WSW to NW-SE-trending dykes, ranging from 0.02 to 2 m in thickness, and from 1 to 130 m in length. Dykes thinner than 1 m and shorter than 10 m predominate, but true length is difficult to measure due to soil cover and vegetation.

The Resende lamprophyres can be classified as alkaline lamprophyres (camptonite, mochiquite, and sannaite) based on their petrographic features (Streckeisen and Le Maitre 1979, Le Bas and Streckeisen 1991, Rock 1991, Woolley *et al.* 1996, Le Maitre 2002, Tappe *et al.* 2005). Table 2 shows the modal composition of 11 alkaline lamprophyres exhibiting characteristic Mg-rich phenocrysts, castellated and pseudohexagonal phlogopite (Fig. 3F), panidiomorphic texture, glass and ocelli, all lacking feldspar phenocrysts.

The less altered to unaltered lamprophyres in the study area are dark purple (Figs. 3G and 3H), holomelanocratic and exhibit porphyritic to glomeroporphyritic, panidiomorfic, and/or poiquilitic textures with euhedral, hydrous, and anhydrous mafic phenocrysts involved in a fine-grained groundmass (Fig. 4). Augite is the most abundant phenocryst, followed by kaersutite and biotite-phlogopite, as well as olivine (that does not appear in some intrusions). Augite and olivine exhibit disequilibrium textures such as resorption, embayment, and zoning. The groundmass is formed by the same minerals as the phenocryst assemblage and variable amounts of plagioclase, analcite and/or glass. Opaque minerals and apatite are also part of that microcrystalline groundmass. Carbonate- and/or silicate-infilled, subrounded ocelli ranging from 0.5 mm to 1.5 mm in size occur in some lamprophyres. Biotite-phlogopite and kaersutite occupy the core of the ocelli but appear more frequently as tangential crystals. Main alteration products include opaque minerals, iddingsite and serpentine.

Camptonites

The camptonites are melanocratic glomeroporphyritic rocks with euhedral augite and olivine as main phenocrysts. The groundmass comprises augite, olivine, opaque and lath-shaped minerals such as plagioclase, kaersutite and smaller amounts of biotite and apatite. Interstitial glass is rare; however, ocelli, xenoliths and xenocrysts of felsic phases are frequent.

Augites range from 0.2 to 5 mm, being found as phenocrysts as well as in the groundmass. The former is euhedral with

concentric zoning with euhedral pinkish rims and anhedral resorbed green cores (Fig. 4E). Clinopyroxene clusters often present olivine inclusions. Some of the microphenocrysts also present corroded rims, suggesting instability and disequilibrium processes. Pseudomorphic olivine crystals range from 0.2 to 1.8 mm and occur more often as phenocrysts.The irregular

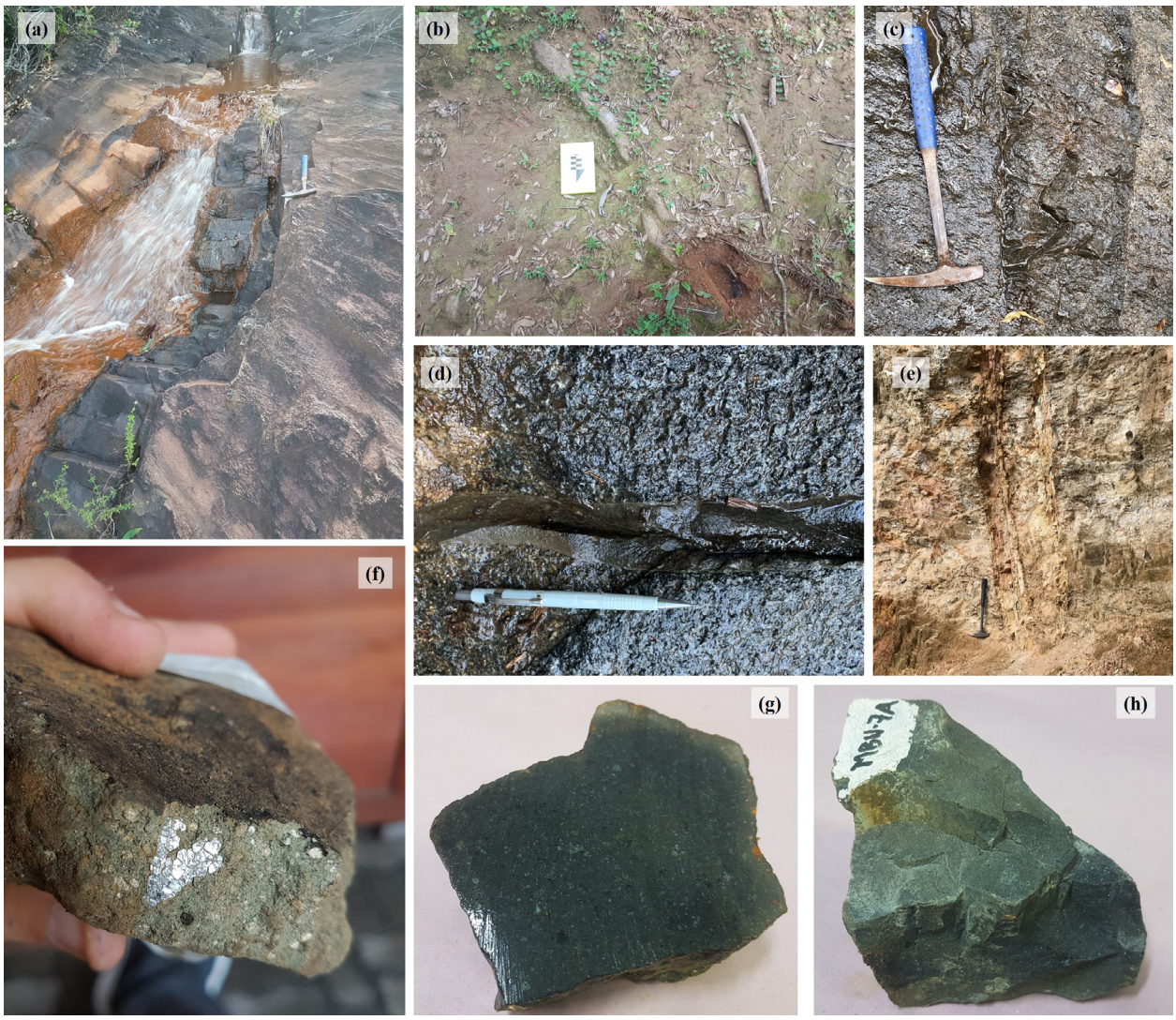

Figure 3. Photographs of outcrops with lamprophyre dykes (a-e) and hand specimens (f-h). (A) Segmented WNW-trending lamprophyre (monchiquite) dyke crosscutting a ENE-WSW mylonite (point MBN 66, this work; point RE-39b; Guedes *et al.* 2005); (B) NW-oriented camptonite intrusion (point MBN-1; (C) Phlogopite-rich dyke (MBN-75) firstly visited by Ferroni *et al.* (2018). This outcrop shows a WNW-trending zigzag dyke; (D) Thin mafic dyke (MBN-65) on same position as mica-rich lamprophyres (94SOB97; Thompson *et al.* 1998); (E) Two ENE-WSW parallel altered alkaline lamprophyres forming red-brown material with less altered biotite (MBN-75); (F) Less altered, pseudohexagonal phlogopite within altered groundmass of lamprophyre (monchiquite MNB-44); (G) Unaltered, porphyritic lamprophyre (camptonite MBN-01). H) Typical aphanitic texture of lamprophyres in the study area (monchiquite MBN- 07A).

Table 2. Modal composition (vol. %) of the less altered and unaltered Resende lamprophyres. Accessory + secondary: apatite (primary), iddingsite, serpentine, chlorite.

Classification	MBN-1	MBN-5	MBN-6	MBN-7	MBN-10	MBN-11	MBN-13	MBN-34	MBN-36	MBN-41	MBN-44
	Camptonite	Sanaite	Monchiquite	Monchiquite	Monchiquite	Monchiquite	Monchiquite	Camptonite	Monchiquite	Monchiquite	Monchiquite
Olivine	9	18	2	2	10	11		11	2		
Clinopyroxene	26	24	10	20	14	30	27	24	17	10	13
Feldspars	18	8		9	8	7		16		8	5
Amphibole (Ksr)	5	4	4	17	21	5	3	7	20	11	10
Biotite (Phl)	8	11	26	14	7	19	19	9	8	32	38
Glass	5	15	38	22	28	12	31	6	37	10	18
Opaque minerals	11	12	15	5	8	15	15	9	4	2	4
Accessory + secondary	12	8	2	9	4	1	5	9	12	27	12
Xenoliths/ xenocrysts	6	0	3	2				3			

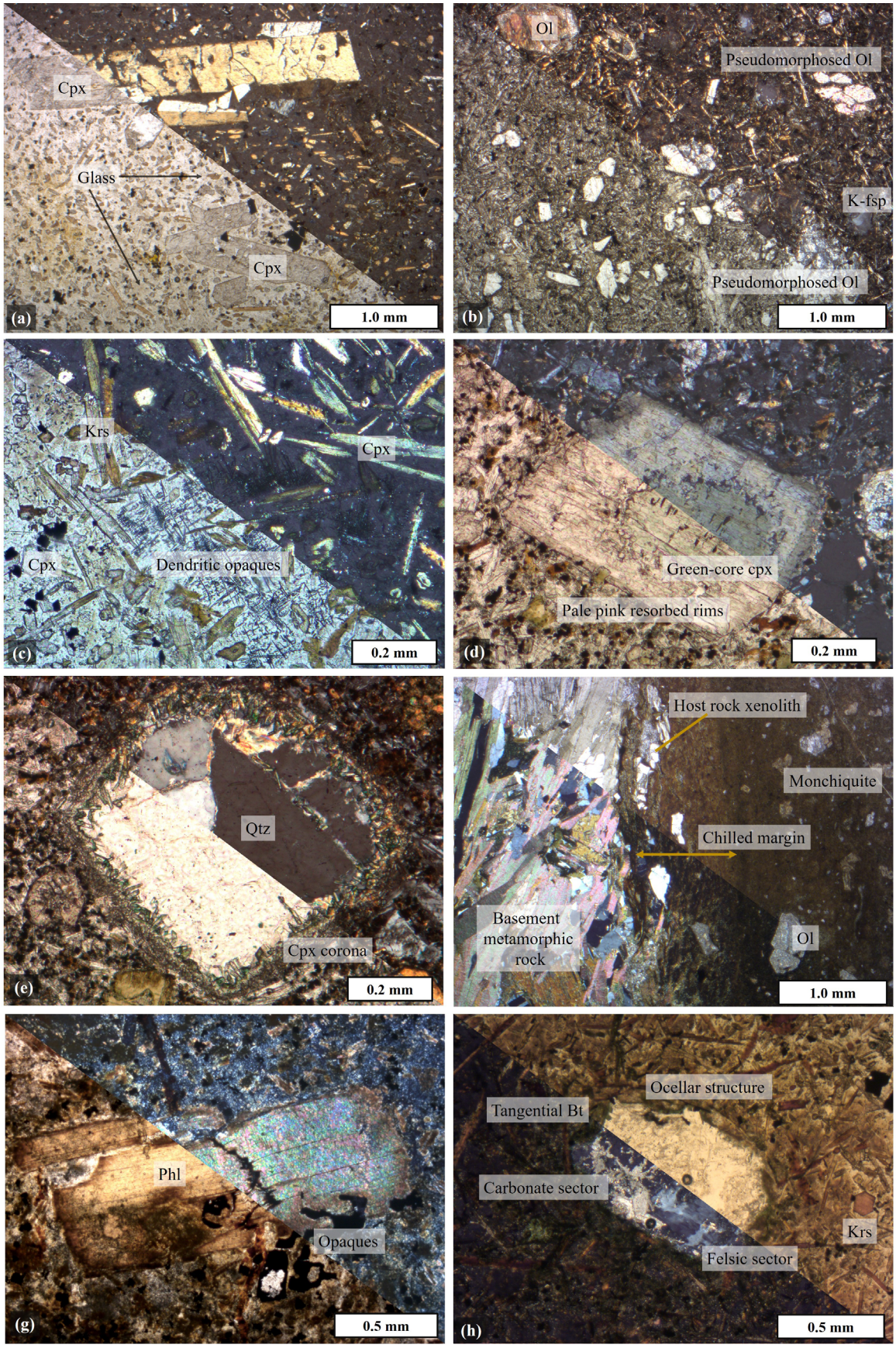

Figure 4. Main petrographic features of the studied Resende lamprophyres. Abbreviations from Whitney and Evans (2010). Photomicrographs under parallel and crossed nicols (below and above diagonal). (A) Porphyritic monchiquite (sample MBN-36) with euhedral clinopyroxene phenocryst surrounded by a groundmass composed of clinopyroxene, amphibole and glass. (B) Glomero-porphyritic sannaite with clusters of olivine pseudomorphs (iddingsite and serpentine alteration products) and alkalifeldspar (k-fs) within the groundmass (sample MBN-05). (C) Detail of the monchiquite groundmass showing kaersutite (krs) and clinopyroxene (cpx) laths, and dendritic opaque minerals surrounded by glass (sample MBN-7). (D) Green-core clinopyroxene on camptonite (sample MBN-01). Note the resorbed rims. (E) Quartz xenocryst surrounded by cpx corona in camptonite (sample MBN-34). (F) Chilled margin contact between metamorphic gneiss and monchiquite with microxenoliths (sample MBN 07). (G) Kink banded phlogopite phenocryst in altered monchiquite with opaque minerals (sample MBN-41). (H) Monchiquite with ocelli composed of carbonate and felsic phases with tangential biotite (MBN-13).

fractures in the olivine are filled by secondary iddingsite. However, fully preserved olivine coexists with pseudomorphs and show no signs of alteration.

The groundmass comprises plagioclase laths (0.1 mm), opaque minerals, kaersutite, interstitial glass and ocellar structures. Ocellar structures range from 0.5 mm to 2 mm and are filled by carbonate, usually in the central portion, with analcime and acicular kaersutite at the contacts with the groundmass. Quartz xenocrysts are common (Fig. 4E), always appearing surrounded by a clinopyroxene corona growing towards the core of the xenocryst. Less frequently, xenoliths of medium-grained metamorphic rocks composed of quartz, feldspar, pyroxene, and opaque minerals are easily distinguished from the enclosing lamprophyre due to its felsic mineral abundance and alteration rims (Fig. 4F). There are also minor amounts of coarse-grained clusters of pale green clinopyroxene with inclusions of olivine and opaque minerals.

Monchiquites

Monchiquites are dark purple holomelanocratic porphyritic rocks with panidiomorfic texture and aphanitic groundmass (Fig. 4A). Chilled margins (Fig. 4F) occur more frequently on monchiquites than the narrower camptonites and sannaites. Phenocrysts include large amounts of euhedral augite or biotite-phlogopite), and minor contents of kaersutite. The olivine is scarce, being restricted to the phenocryst assemblage, always fractured, and rimmed by secondary opaque minerals. The monchiquite differs from the camptonite in its higher glass content, where all crystal phases are immersed. Ocellis present a sharp contact with the groundmass and display a sub-circular shape.

Euhedral clinopyroxene crystals range from 0.05 mm to 5 mm and share the same petrographic features, occurring as isolated well-formed crystals or as radial clusters. Augite presents hourglass and concentric zoning with beige colors on its center and pinkish thin rims, with an anomalous blue interference. Kaersutite, opaque minerals and apatite are the most common inclusions on clinopyroxene. Olivine pseudomorphs are characterized by elongated fractures within euhedral crystals that are partially or entirely altered to iddingsite and serpentine.

Biotite-phlogopite and kaersutite form macro and microphenocrysts with distinctive features. Biotite-phlogopite present needle-like, castelled, and pseudohexagonal shapes. Bent or kink-banded crystals also occur (Fig. 4G). The kaersutite is euhedral and shows embayment with groundmass filling the gaps whereas euhedral opaque minerals frequently occur as dendritic clusters (Fig. 4C). Ocelli are circular to ellipsoidal and have sharp contacts with the groundmass, filled by carbonate and felsic phases with no regular pattern (Fig. 4H). Needle-like kaersutite and tangentially distributed biotite-phlogopite are present in almost all ocelli structures. Glass (Fig. 4C) comprises 12% to 38% of modal volume in monchiquites.

Sannaite

The occurrence of K-feldspar as the main felsic phase is the distinguishing petrographic feature of the sannaites (Fig. 4B). The sannaites are dark grey holomelanocratic rocks with a glomeroporphyritic, panidiomorphic texture, composed of partially or completely altered coarse-grained olivine phenocrysts and unaltered augite set in an aphanitic groundmass. A fine-grained groundmass is composed of the same phases as the phenocryst assemblage with added biotite, k-feldspar, opaque minerals, interstitial glass and ocellar structures. Sannaites display intracrystalline fractures that are filled by carbonate and other secondary phases.

Olivine glomerophenocrysts reach 5 mm in size and can be composed of several crystals that are partially or completely altered to serpentine. Microcrysts preserve the same features, but isolated crystals are more common. The clinopyroxene is 0.2 to 2 mm and comprises macrocrysts and microcrysts with beige cores and pink rims. Intergrowths and radial patterns are common. Hourglass and concentric zoning are also present.

K-feldspar is present only in the groundmass forming subrounded grains (0.2-0,5 mm), and ocelli are filled by carbonates with tangential kaersutite and biotite-phlogopite. Euhedral opaque minerals rarely form phenocrysts (1 mm); in addition, they occur more frequently as small crystals and mainly as dendritic shapes in the groundmass. Interstitial glass fills the gaps between all crystalline phases.

Whole-rock chemistry

New lithogeochemical data obtained for 6 samples of the Resende lamprophyres are presented (Tab. 3) and analyzed with compiled data of 19 samples of lamprophyres that occur in the study area (Suppl. Tab. 1; Riccomini *et al.* 1991, Thompson *et al.* 1998, Guedes *et al.* 2005, Marins 2012, Brotzu *et al.* 2005).

They are ultrabasic/basic alkaline rocks chemically classified as basanites, tephrites and foidite, except for one more evolved phonotephrite (Fig. 5). The Resende lamprophyres present low SiO_2 contents (47.20-28.50 wt.%), high contents of TiO_2 (2.51-5.23 wt.%), and variable amounts of Al_2O_3, CaO, K_2O, and Na_2O (10.37-19.5; 5.40-13.39; 0.71-8.50 and 0.52-4.65; wt.%, respectively). MgO and Cr contents range from 3.18 to 10.57 wt.% and 5 to 610 ppm respectively. Mg-number (Mg#), Ni and Sc present a wide variation (36-59 ppm; 25-200 ppm; 16-26 ppm, respectively). The extensive range of Mg# and compatible elements variation suggest that the lamprophyre magmas in the study area may have undergone magmatic differentiation and some dykes may represent the primitive material.

The CaO *versus* Al_2O_3 discrimination diagram (Fig. 6A) confirms that the Resende alkaline mafic dykes are lamprophyres as opposed to lamproites or kimberlites, whereas the TAS diagram also certifies that these rocks are alkaline lamprophyres. All but two samples plot in the alkaline lamprophyre field, the latter being classified as ultramafic lamprophyres. Alkalis ratios (K_2O/Na_2O) range between 0.33 to 4.14, *i.e.*, there are sodic, potassic and ultrapotassic lamprophyres in the study area (Fig. 6B). The new data presented in this paper increase the range of sodic and potassic types and introduce ultrapotassic rocks to the Resende regional ultramafic-mafic alkaline magmatism. The alkaline lamprophyres are olivine, diopside and nepheline normative rocks without normative quartz. Average CaO contents (10.0 wt.%) areclose to average in alkaline lamprophyres worldwide (10.3 wt.%; Rock 1991).

High values of loss on ignition (LOI; 1.24-13.13 wt.%) and CO_2 (2.70 and 3.80 wt.%) coupled with the presence of kaersutite, biotite-phlogopite and carbonates are typical features of alkaline lamprophyres worldwide, and indicate a volatile enrichment not necessarily related to secondary alteration. Although high LOI values are intrinsic to lamprophyres, two samples (MBN-10 and AGN-GM-05D) with anomalously low SiO_2 contents (28.50 and 31.95) present LOI above 10

Samples	**MBN-01**	**MBN-05**	**MBN-07**	**MBN-10**	**MBN-34**	**MBN-36**
Rock type	**Camptonite**	**Sannaite**	**Monchiquite**	**Monchiquite**	**Camptonite**	**Monchiquite**
SiO_2	43.40	39.90	47.20	28.50	44.90	40.50
TiO_2	2.51	3.82	2.97	5.23	2.71	3.93
$Al2O_3$	12.60	11.80	17.25	17.25	14.80	19.50
Fe_2O_3	11.55	13.45	7.78	19.15	11.60	10.20
MnO	0.19	0.27	0.18	0.20	0.19	0.21
MgO	9.57	7.52	3.18	5.81	7.74	3.98
CaO	10.85	10.25	5.40	7.09	10.25	6.21
Na_2O	2.64	3.04	2.05	0.52	3.54	1.19
K_2O	1.85	1.99	8.50	0.71	2.49	4.76
P_2O_5	0.89	0.80	0.75	1.29	1.02	0.92
LOI	2.51	5.87	3.84	12.25	1.56	8.46
Total	99.01	99.21	99.55	98.24	101.24	100.26
Cs	6.6	165.0	4.8	0.7	0.6	1.6
Rb	54.7	188.5	279.0	20.5	54.3	164.0
Ba	1415	2630	1890	1350	1635	1945
Th	7.40	9.84	16.35	13.20	9.81	17.40
U	1.63	2.38	4.18	3.34	2.30	4.16
Ta	7.0	6.4	9.3	8.0	6.9	10.0
Nb	82	107	148	128	103	171
Sr	1650	1005	1780	752	1810	1340
Zr	250	450	517	498	349	590
Y	33.8	30.5	42.5	44.4	39.8	45.5
Cr	610	560	50	30	310	70
Sn	3	4	3	4	6	4
Ga	17.5	21.6	26.7	32.8	20.4	28.8
Hf	5.8	9.8	10.5	11.9	7.3	11.7
W	2	4	3	2	2	1
V	268	316	183	405	241	244
La	102	88	130	109	135	140
Ce	185	174	235	211	214	263
Pr	22.4	20.8	26.9	25.3	24.8	30.1
Nd	77.8	77.0	94.2	98.0	88.2	106.5
Sm	12.0	13.1	14.6	17.1	14.2	17.6
Eu	3.54	3.34	3.97	5.22	4.10	4.88
Gd	8.86	9.69	11.60	13.40	10.25	12.40
Tb	1.31	1.23	1.71	1.82	1.39	1.71
Dy	6.35	6.08	7.92	9.19	7.51	8.67
Ho	1.19	1.17	1.49	1.71	1.39	1.58
Er	2.93	2.55	3.50	3.94	3.55	3.85
Tm	0.42	0.38	0.50	0.53	0.49	0.52
Yb	2.54	1.91	2.72	2.83	2.84	2.87
Lu	0.36	0.27	0.39	0.42	0.40	0.39

wt.%, indicating possible alteration. These are the two samples that plot in the UM field and their geochemical data may not reflect magmatic processes. Thus, they will not be considered in the petrological discussion.

The variation diagrams with MgO as a differentiation index can be found in Fig. 7. The MgO and CaO contents yield higher values for samples with higher proportions of modal olivine and clinopyroxene. The Cr curve follows a decreasing trend towards the most evolved samples that may be related with clinopyroxene fractional crystallization. This relationship is corroborated by the lower content of modal clinopyroxene as phenocrystals in the more evolved ultrapotassic lamprophyres. In sodic and potassic lamprophyres, clinopyroxene and olivine make up most of the rock, exclusively as phenocrysts. The CaO/Al_2O_3 decreasing rates is also consistent with clinopyroxene fractionation. Despite scattering, the overall increase in the contents of SiO_2, Na_2O and K_2O is also consistent with a major control of mafic phases (clinopyroxene and possibly olivine) during the fractional crystallization processes. There is no evidence for feldspar fractionation as expected for lamprophyres. The abundance of modal opaque minerals (avg.,

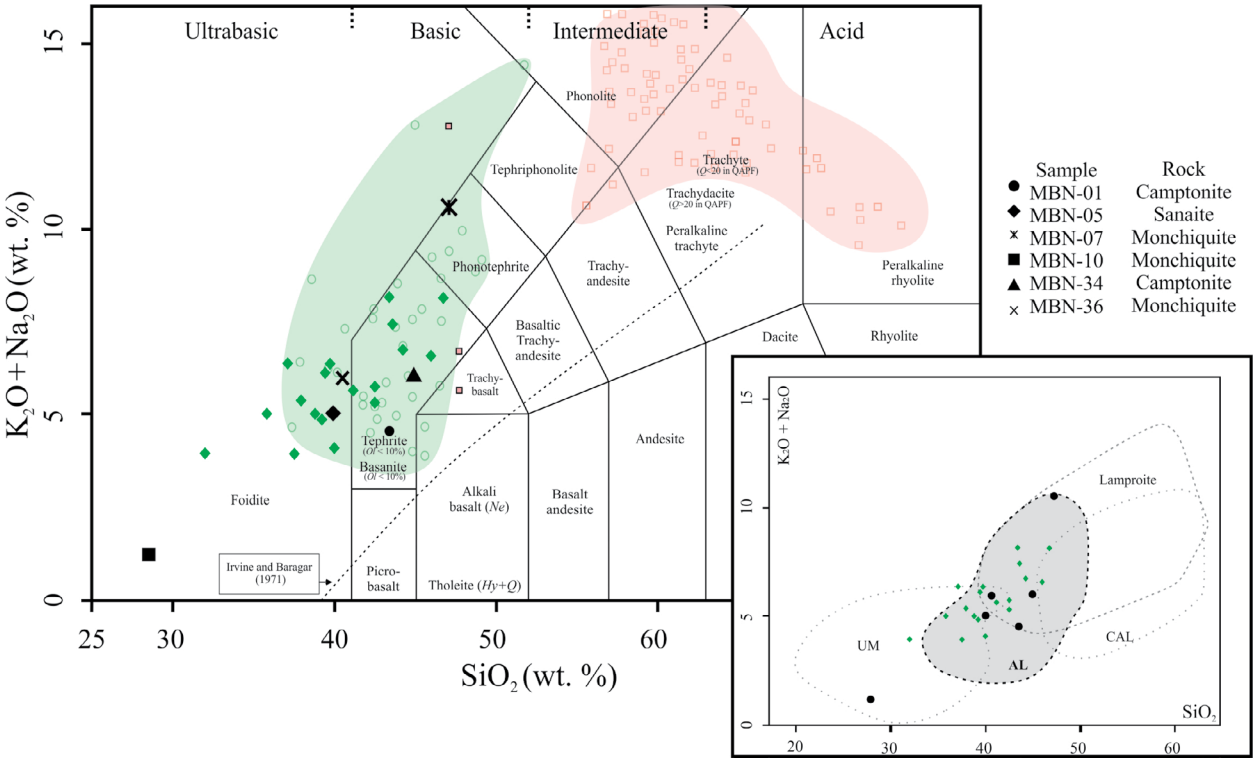

Figure 5. TAS diagram (Le Bas *et al.* 1986) showing herein presented dykes (black icons) in an alkaline ultrabasic/basic trend. Green diamonds represent previous data from the Resende lamprophyres, compiled from Riccomini (1989), Thompson *et al.* (1998), Guedes *et al.* (2005), Marins (2012). Pale green (circles with pale green edges represent the samples) and red (squares with pale red edges represent the samples) background field are related to geochemical data from regional lamprophyres along CFMA and IAM rocks (Brotzu *et al.* 1997, Marins 2012, Melluso *et al.* 2017, Rosa 2017), respectively. Both data can be found in Suppl. Tab. 1 and Suppl. Tab. 2. Pink filled squares with black edges represent mafic rocks from IAM (Rosa 2017). Lamprophyre types and Lamproite fields from Rock (1991).

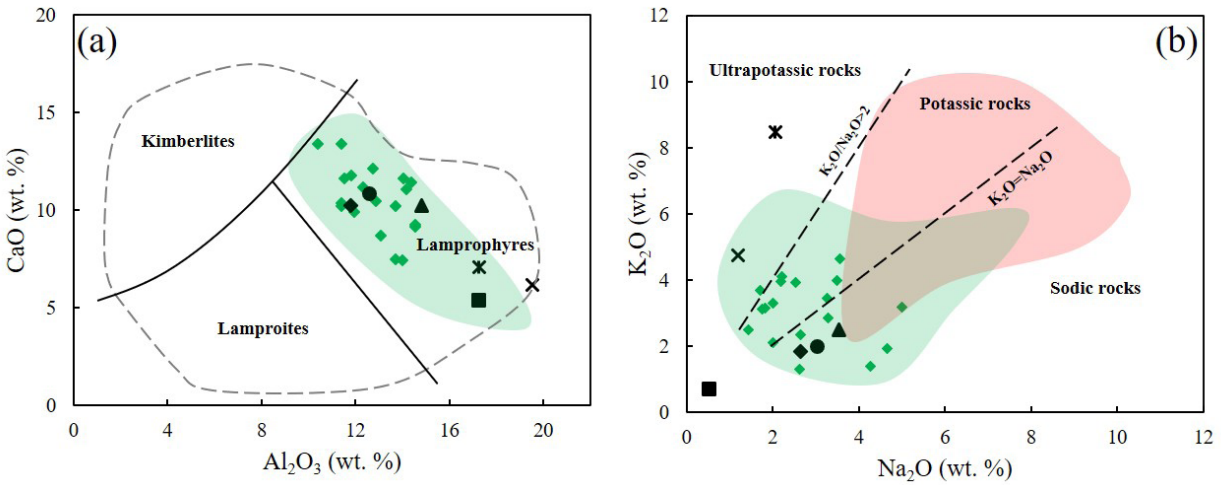

Figure 6. The Resende lamprophyres plotted in discrimination and classification diagrams. (A) CaO versus Al_2O_3 discrimination diagram for kimberlites, lamproites and lamprophyres (Foley *et al.* 1987). (B) Na_2O versus K_2O classification diagram for ultrapotassic, potassic and sodic rocks. Lines from Foley *et al.* (1987) and Orejana *et al.* (2008).

10%) is represented by the high values of TiO_2 (> 2.5 wt.%) and Fe_2O_3 (usually > 10 wt.%). The Resende lamprophyres are richer in TiO_2 when compared with the lamprophyre dykes from other swarms in Rio de Janeiro (*e.g.*, Valente 1997). The Resende dykes also display a scattered distribution of TiO_2, ranging between 2.51 and 5.23, as well as preventing the classical discrimination between groups of high or low TiO_2 (*e.g.*, Gibson *et al.* 1995).

The chondrite-normalized rare earth element (REE) diagram shows a steep linear pattern with enrichment in LREE; between 100 to 500 times the chondrite values (Fig. 8A). The $(La/Yb)_N$ values vary between 24.9 to 38.1. Only few samples yield lower $(La/Yb)_N$ ratios, ranging from 15 to 17 and one sample (MBN-66/RE-39b; Guedes *et al.* 2005) presents an extremely high $(La/Yb)_N$ ratio (63.8). In general, the ultrapotassic and some of the evolved potassic lamprophyres tend to yield $(La/Yb)_N$ ratios above 30. The lack of Eu anomalies (Eu/Eu* = 0.91 to 1.16) also precludes feldspar as a fractionation phase as expected for lamprophyres which lack feldspar phenocrysts by definition (Rock 1991). The newly studied samples in the Resende lamprophyre swarm display parallel to sub-parallel patterns in the primitive mantle-normalized multielement diagram (Fig. 8B). The main features are troughs when it comes to Th, U, Sr, P, and Zr, and peaks for Ba and Nb. Decoupling between Nb and Ta may be related to crushing in the WC mill. The Sr, P and Zr negative anomalies may be related to residual accessory phases in the mantle sources. The $(La/Nb)_N$ ratios < 1 and $(La/Yb)_N$ ratios > 1 shown in the multielementar diagrams (Fig. 8B) indicate that the Resende lamprophyres are likely to be a fertile, OIB-like mantle.

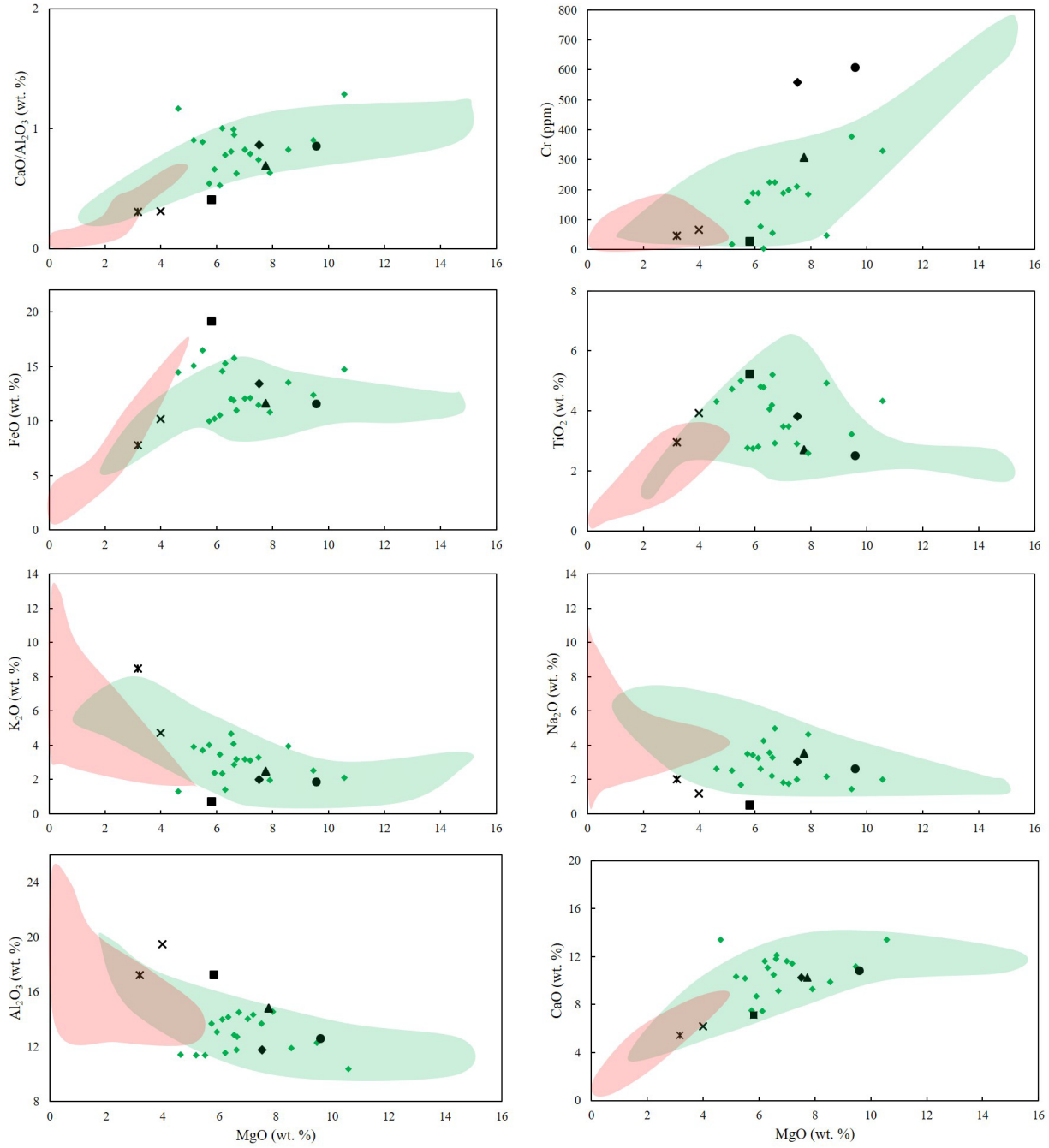

Figure 7. Variation diagrams for the Resende lamprophyres. Oxides in wt.%. Elements in ppm. Symbols and fields as in Fig. 5.

Structural model

Geometrical analysis

The basement is formed by anisotropic metamorphic rocks, such as amphibolite, quartzites, gneisses and mylonites. An ENE-WSW trending regional foliation is constant and occurs on almost all lithologies (Fig. 9). Dip angle average is close to 60° in the SSE direction, but some shear zones increase its dip angle close to 90°. Regardless, these zones maintain the foliation strike. Brittle structures cross-cutting the basement rocks encompass quartz-tourmaline veins, joints, and tholeiitic dykes. The former are thin intrusions (ca. 4 cm wide) trending WNW to NE directions. Joints are linear and regular structures that predominate in the WNW-trending direction with sub-vertical dip, although ENE fractures also occur (Fig. 9). Thick and rare diabase dykes (10 m wide) occur as NNE- to NNW-trending intrusive bodies, representing tholeiitic magmatism related to the early stages of the South Atlantic opening. On the field, they are different than lamprophyre bodies due to a higher thickness, presence of feldspar phenocrysts, lack of hydrous mafic phases, plus alteration in color and texture. Therefore, the basement is affected by three clear discontinuity sets. The main set is positioned on the WNW direction followed by an NNE to NE group. Few brittle structures occur on the NNW to NW directions.

Lamprophyre dykes are thin (2.6 cm to 2 m thick) abrupt intrusions that cross-cut country rock and its structures (Fig. 9). Table 4 displays 36 representative measurements from the

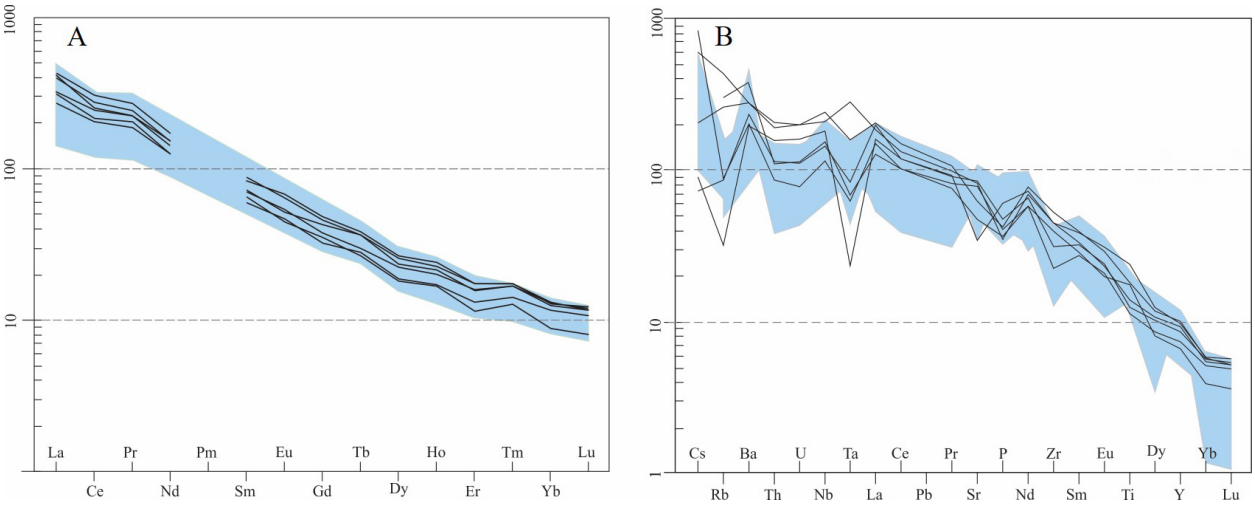

Figure 8. Multielement diagrams for the Resende lamprophyres. (A) Chondrite-normalized REE diagram Normalization values from Nakamura (1974). (B) Primitive mantle-normalized multielementar diagram. Normalization values from McDonough and Sun (1995). The shaded blue areas in both diagrams represent patterns of compiled previous data of the Resende lamprophyres. Samples of the current study in black.

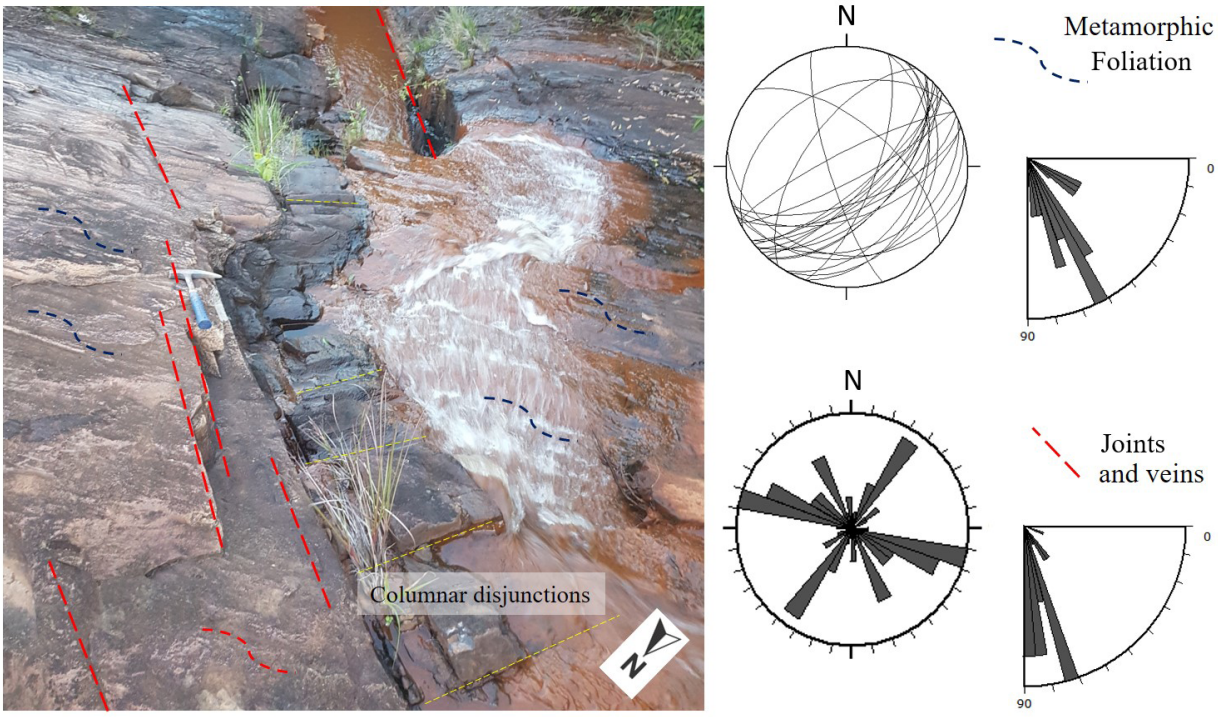

Figure 9. Representative outcrop (MBN-66) showing the common structural framework of basement rocks and its structures. NW-oriented lamprophyre dyke exhibit offsets with dilations.

herein presented dykes. Due to dense vegetation, few meters long bodies predominate. Regardless, there is evidence, such as the presence of lustrous ochre soil, of bodies reaching kilometer lengths (*e.g.* MBN-01). Vertical to sub-vertical outcrops tend to display a regular and continuous intrusion shape, whereas horizontal to sub-horizontal outcrops often exhibit plenty of dyke segmentations. Only one sill was found, intruded on mylonitic quartzite and parallel to its ENE-azimuth and SSE-dipping foliation. The main lamprophyre set follows an ENE vertical to sub-vertical trend, and average dip angle between 75° to 90° and SSE to NNW dip direction, comprising almost all sheet intrusions (36; Fig. 10). These strikes are parallel to the basement foliation, but do not intrude on its previous pathway. In other words, they do not respect prior structures and predominate as vertical to sub-vertical intrusions on this direction even in anisotropic rocks, such as the non-deformed granitoids that present dip angles higher than 60°. Secondary trends are formed by WNW and NW bodies (12) that often emplace previous parallel fractures and comprise all offsets observed, apart from an offset that affects the single ENE sill.

Table 4. Herein presented lamprophyre dyke orientations and size. Pale-grey measurement represents secondary sets. Dark grey represents the main ENE-WSW to NE-SW dyke set.

ID	Thickness (m)	Length (m)	Orientation (Dip/dip)
MBN-01	-	-	45/85
MBN-05	0.45	2	03/85
MBN-06	1	2	10/80
MBN-07	0.45	7	330/45
MBN-09	0.4	2	160/88
MBN-10	0.3	2	165/85
MBN-11	0.15	2	158/85
MBN-13	1	5	140/84
MBN-14	0.2	2	330/80
MBN-15	3	6	55/70
MBN-16	3	5	165/85
MBN-26	0.4	4	112/60
MBN-36	3	1	330/86
MBN-38	0.3	1	178/84
MBN-41	3	100	160/60
MBN-42	1.5	3	185/85
MBN-43	1	1	130/83
MBN-44	0.45	1	110/78
MBN-45	1	1	160/89
MBN-46	1	1	175/88
MBN-48	0.4	1	160/80
MBN-50	0.15	1	340/85
MBN-53	0.15	1	233/75
MBN-62	0.3	35	133/81
MBN-63	0.6	10	152/80
MBN-64	0.5	5	332/76
MBN-65	0.026	3	20/86
MBN-66	0.6	100	33/86
MBN-67	0.12	10	159/65
MBN-70	0.3	1	40/86
MBN-71	0.7	1	234/79
MBN-72	0.6	1	170/85
MBN-73a	0.2	1	175/87
MBN-73b	0.1	1	175/87
MBN-74	0.45	1	330/60
MBN-75	0.30	1	10/85

According to the criteria and structural hierarchy presented by Delaney *et al.* (1986), WNW-ESE dykes may represent intrusions that flow through previous pathways and their main segments cannot be used as good paleostress indicators, due to the abundance of adjacent and regional parallel fractures following this direction. Field relationship confirms that some of the WNW-trending dykes are intrusive on previously parallel fractures. Contrarily, ENE-WSW dykes may represent safe paleostress indicators since there are not plenty of parallel adjacent and/or regional basement joints occurrence at the area, suggesting an NNW-SSE local extension, following the statement that σ_3 is perpendicular to the main dyke wall segmentation. Nonetheless, some of the ENE-WSW bodies could also intrude on previous discontinuities (*e.g.* sill MBN-67).

Kinematic analysis

Bridges, steps, heels, and horns represent the main offset features that affect the main dyke segments. All these structures, as mentioned, are inserted on WNW lamprophyre intrusions (Fig. 10) and are oriented in an NNW- to NW-trending direction (dilation strike). Furthermore, ENE-trending dykes are continuous, whereas WNW display numerous discontinuous offsets. Without exception, offsets that affect WNW dykes maintain a consistent stepping direction (*e.g.* Magee *et al.* 2019). On the other hand, a single ENE sill that shows

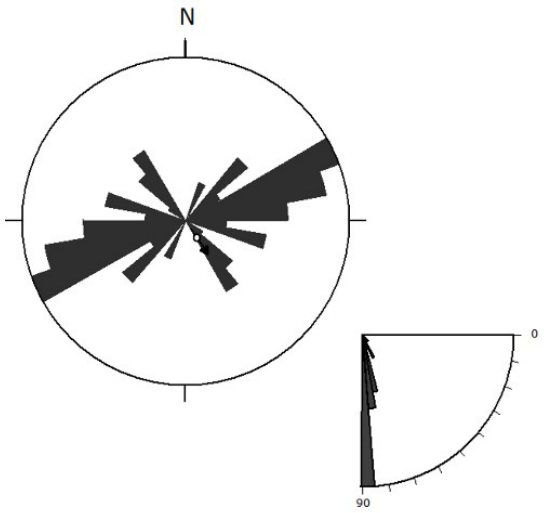

Figure 10. Rose diagram depicting herein presented lamprophyre dyke strikes on the main ENE-WSW oriented set with secondary WNW- to NW-trending group. Note that the overall dip angle ranges between 80° to 90° and the dot does not follow the metamorphic foliation dip angle (ca. 60°).

a bridge and a horn displays an inconsistent stepping direction. Consistent displacements maintain their sense of motion and can be used in extracting the direction of dilations while inconsistent ones cannot be used in this analysis due to the change in sense. It is important to establish that none of these structures are faulted, indicating a non-faults offset, common features on lamprophyres (*e.g.* Rock 1991).

In order to evaluate dilation direction, we applied the Bussel's Method (1989). On the Resende lamprophyres, dilation planes were obtained via measuring apparent direction on consistent stepping dykes (stepped or zigzag patterns) and strike and dip direction of the main dyke segments.

MBN-66 shows one step and one bridge (Fig. 11A), the last one being submerged in a river (Fig. 9); hence it could not be measured. However, it follows the step's consistency. Concerning the step, two sub-horizontal NNW-SSE parallel dilations could be identified by previous adjacent points of country rock. It is relevant to establish that no fault or transcurrent movement occurred, although dextral virtual configuration can be identified. Virtual sinistral configuration was observed on two other offset dykes, where the first one (MBN-65) shows a WNW-trending main segment with steps and a bridge, that also point to a sub-horizontal NNW-SSE dilation direction, formed by three steps (Fig. 11B). The last dyke represents the most important feature for kinematic analysis. A WNW-oriented dyke with a zigzag pattern formed by at least six consistent steps (Fig. 12). Twelve NNW-SSE to N-S sub-horizontal dilations are in consonance to other dilation directions and fits satisfactorily with an NNW-SSE local extension, reaching 16 dilations measured (Fig. 13). According to the Bussel's Method, regional dilation direction can be estimated by the pole of the best suited plane that fits on the whole pole of dilation planes. This pole represents the robust mean of sub-horizontal NNW-oriented minimum principal stress (σ_3) and positions it at an estimated 339/70 (Fig. 13). In this context, the average net dilation of some of the Resende lamprophyres points to a sub-horizontal NNW-SSE local extension that fits with preliminary geometrical analysis and correlates with a possible least compressive stress axis (σ_3) on this direction.

Furthermore, one normal fault was observed with a branched lamprophyre dyke inserted on the fault plane (Fig. 14). Both structures show an ENE-oriented strike and an 80° dip angle to the SSE direction. A sub-parallel branch and the presence of SSE-dipping slickensides (striated clay minerals), either on the main or the secondary segment, suggest a contemporaneous relationship between the fault and the dyke pointing to a possible NNW-oriented extensional regime as the main control, similar to the aforementioned analysis (NNW-SSE extension).

Paleostress from fracture/fault slip inversion

Dyke walls, slickensides/slickenlines and fault plane data were produced via field measurement and grouped with similar geometrical and spatial characteristics. Afterwards, they were analyzed by the WinTensor software (Deulvax and Sperner 2003) based on the fault slip inversion method (Angelier 1991, 1994). Despite the scarcity of fault plane and slickensides data, and the limited occurrence of dilation planes, a paleostress estimative was produced. As the Resende dykes form groups with orthogonal patterns and no oblique features, they may represent kinematically incompatible sets, therefore, they were analyzed separately. The main ENE-WSW segments were plotted together with the parallel unique fault plane and its slickensides (dipping SSE) due to kinematic compatibility, while the WNW-ESE and NW-SE dyke walls were grouped together in a separated analysis.

A deformational model was built considering only the main segments of the dykes. According to the WinTensor

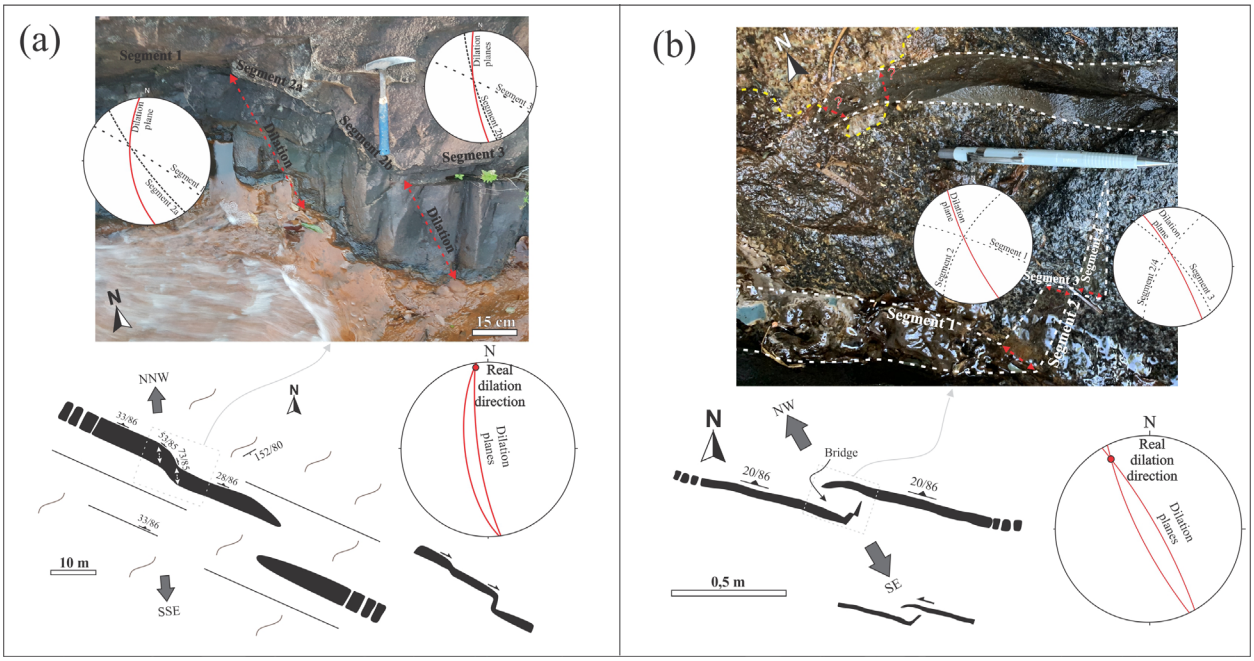

Figure 11. The direction of the dilations (NNW to NW) are different from the main segment opening (NNE-NE). (A) Two dilations (NNW-SSE) on an offset WNW-trending dyke (MBN-66). Note that this dyke encompasses a bridge with the consistent stepping direction. (B) Few dilations showing the same direction (NW-SE) in a consistent stepping direction.

analyses (Fig. 15), the principal dyke set (ENE-WSW) was emplaced by a directional extension regime, with sub-vertical maximum principal stress (σ_1) on 198/81 and sub-horizontal minimum principal stress (σ_3) on 337/07. Subordinated WNW-ESE and NW-SE sets analysis present a pure extension regime, with σ_1 and σ_3 also in sub-vertical and sub-horizontal axis, respectively, but with different azimuth (54/87 and 216/03). These analyses confirm the kinematic incompatibilities of these two groups. In addition, the first deformational model is kinematically compatible with the field observations and previous structural analysis, including average dilation direction, and is therefore more likely to represent the stress responsible for this dyke swarm emplacement, an extensional regime with a NNW-SSE extension as its minimum principal stress (σ_3). Moreover, WNW-ESE and NW-SE secondary sets do not encompass good paleostress indicators according to Delaney *et al.* (1986). Therefore, the NNW-SSE extension represents a more reliable model. This representation will be used for discussions regarding regional magmatic-tectonism.

DISCUSSION

Petrological aspects

General features

The high LOI is a characteristic concerning the lamprophyres worldwide, even in unaltered samples (*e.g.* Rock 1991, Hauser *et al.* 2010, Jiang *et al.* 2010). It is also known that the Resende alkaline mafic dykes are usually affected by secondary alteration (Brotzu *et al.* 2005). Nevertheless, the Resende lamprophyres do not present positive systematic correlations between LOI and mobile elements such as K, Rb and Na (Fig. 16), a typical feature expected in samples affected by post-magmatic alteration (*e.g.* Pouclet *et al.* 2017). Overall, the high LOI values of the Resende lamprophyres can be explained by their high contents of primary volatiles (CO_2 and H_2O).

Liquid immiscibility (silicate and carbonate phases) is often pointed out to explain the presence of ocelli (*e.g.* Cooper 1979, Alves 1997, Alves and Gomes 2001, Nédli and Tóth 2007, Azzone 2008, Scarrow *et al.* 2011, Stoppa *et al.* 2014). The Resende lamprophyres display such features with distinctive

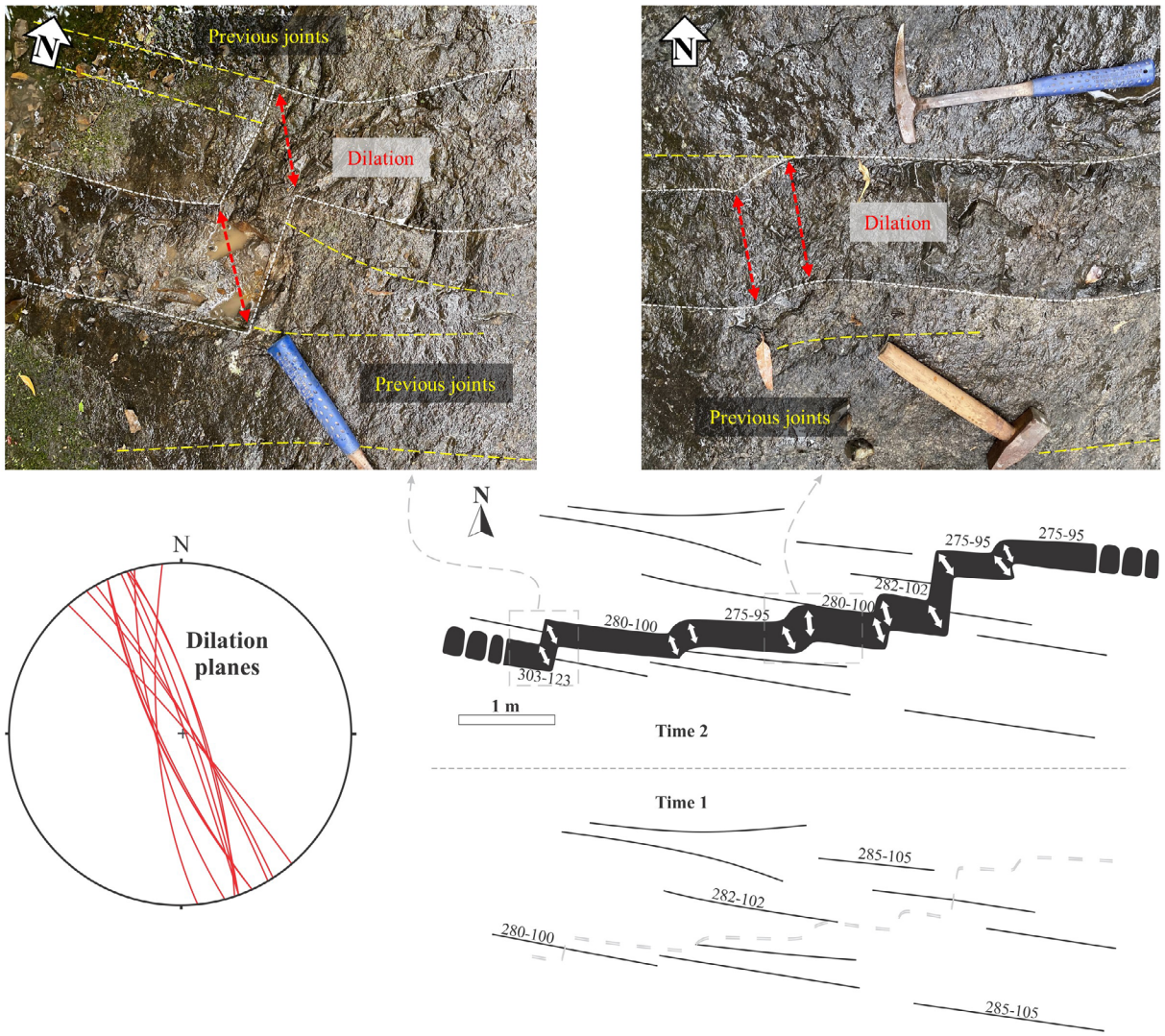

Figure 12. Zigzag lamprophyre dyke with consistent pattern parallel to previous basement joints. Several dilations direction show an NNW-oriented extension, while main dyke segments are supposed to have an NNE extension. Despite the presence of mylonitic foliation on an ENE-WSW direction, only WNW-ESE joints were exploited by lamprophyre magma.

sub-rounded shapes formed by carbonate and analcime, surrounded by or involving hydrous mafic phases. Observed features seem to be also consistant with the late crystallization of either plagioclases or biotite and kaersutite that surround ocelli in some dykes. The variable amounts of the hydrous ferromagnesian minerals around ocelli in some dykes confirm that in addition to CO_2, H_2O was also a volatile phase of the lamprophyre magmas. The Sr negative anomaly shown by the Resende lamprophyres (Fig. 8B) may represent at least partially the presence of residual clinopyroxene and/or carbonate in their mantle sources (Gibson *et al.* 1995). In fact, some Resende lamprophyres (RE-06 and RE-07; Riccomini *et al.* 1991) present high CO_2 contents (between 2.5 and 4.0 wt.%) that cannot be attributed to post-magmatic alteration. Therefore, in addition to fractional crystallization, most of the clinopyroxene and possibly also olivine, as aforementioned, may also have been involved in immiscibility processes between H_2O-rich silicate and CO_2-rich carbonate phases. Rapid cooling is another common feature that frequently appears as a diagnostic lamprophyre characteristic (*e.g.* Rock 1991). In

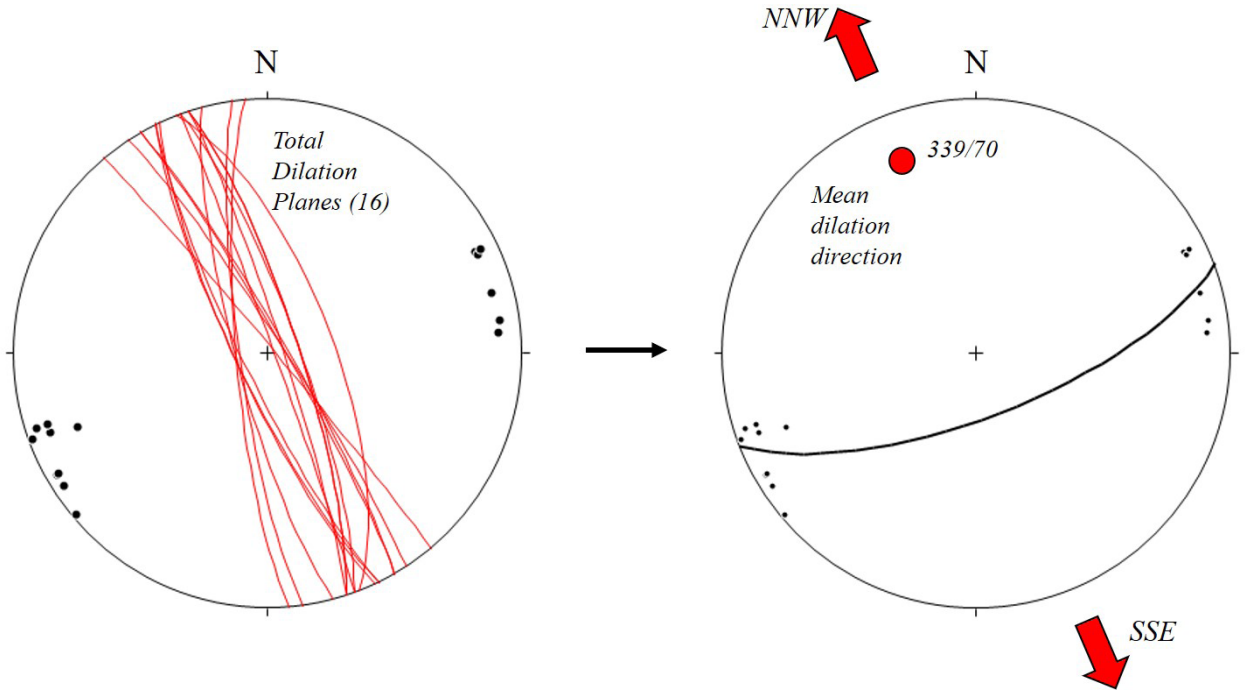

Figure 13. Total dilation planes and its average dilation direction, showing a regional NNW-SSE extension resulted from the Bussel's Method (Bussel 1989).

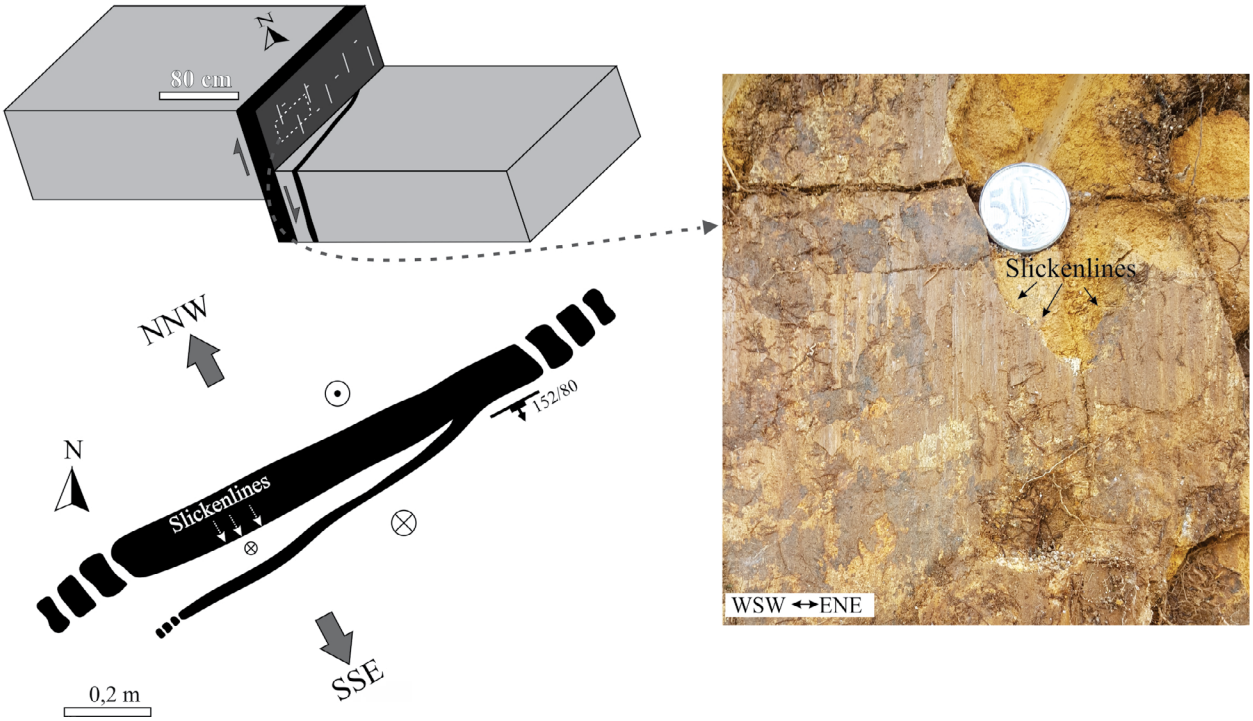

Figure 14. Schematic illustration of lamprophyre dyke inserted on fault plane (ENE-WSW dipping SSE) and preserved slickenlines confirming a dip-slip normal fault.

some of the lamprophyres here presented, chilled margins and dendritic minerals can be found, representing features related to this process.

The presence of crustal xenoliths and xenocrysts in the Resende lamprophyres is evidence of magma and country rock interaction. Nevertheless, there is no abrupt increase in SiO_2 and Al_2O_3 (wt.%) contents that support significant assimilation effects (*e.g.* Pandey *et al.* 2017). This large increment would be expected in quartz-feldspathic mylonite assimilation, the most common metamorphic rock in the study area. The lithophile element Th is heavily concentrated in the continental crust as opposed to the mantle. Therefore, the Th/Ce (< 0.07) and (Th/La (< 0.24) ratios of the Resende lamprophyres preclude expressive crustal assimilation (*e.g.* Raeisi *et al.* 2019). The reaction coronas observed in all xenocrysts may represent a protective shield that prevents the material from being fully assimilated by the lamprophyre magma (*e.g.* Nédli and Tóth 2007). Thus, the partial consumption of subrounded xenocrysts may not have contributed to significant changes in the chemical composition of these lamprophyre dykes. Gneisses xenoliths also occur with similar coronas, confirming an interface between the xenoliths and the groundmass that possibly prevents effective assimilation. Overall, the current discussion corroborates the Sr-Nd isotopic ratios of some of the Resende lamprophyres that indicate that crustal assimilation was not an extensive process in the evolution of those magmas (*e.g.* Thompson *et al.* 1998 — 87Sr/86Sri 0.704-0.705; 143Nd/144Ndi 0.512).

Based on petrographic features, major elements data and parallel to sub-parallel REE patterns, it is likely that these rocks have undergone fractional crystallization. The higher proportion of modal biotite-phlogopite and kaersutite as opposed to clinopyroxene and olivine as phenocrysts in ultrapotassic types and the inverse relationship in Na_2O/K_2O, coupled with decreasing patterns of MgO, CaO and Cr, and increasing SiO_2, Al_2O_3, and K_2O with progressive differentiation (decrease in Mg#), corroborate for the occurrence of fractional crystallization. Differentiation may have involved mostly clinopyroxene and olivine as the main fractionating phases. The absence of Eu (Eu/Eu*) anomaly corroborates to the absence of feldspar in the fractionation process and possibly also as a residual phase in the mantle source (*e.g.* Stemprok *et al.* 2008, Soder *et al.* 2016, Phani *et al.* 2018). Clinopyroxene and olivine fractionation was also proposed for lamprophyres in alkaline provinces of SE Brazil (*e.g.* Garda 1995, Valente 1997, Thompson *et al.* 1998, Brotzu *et al.* 2005, Azzone *et al.* 2018) and elsewhere (*e.g.* Ngounouno *et al.* 2003, Nédli and Tóth 2007, Ubide *et al.* 2012). Despite the low effectivity of crustal contamination, there is evidence that confirms the occurrence of this process (*i.e.* country rock xenocrysts and xenoliths). As previously stated, it is possible that the Resende basanitic/tephritic dykes represent the mafic parental melts of more evolved felsic alkaline stocks (Valença *et al.* 1983, Brotzu *et al.* 1989, Brotzu *et al.* 1997, Brotzu *et al.* 2005, Enrich *et al.* 2005, Riccomini *et al.* 2005, Rosa 2017, Ferroni *et al.* 2018), such as IAM and Morro Redondo during an extensive differentiation

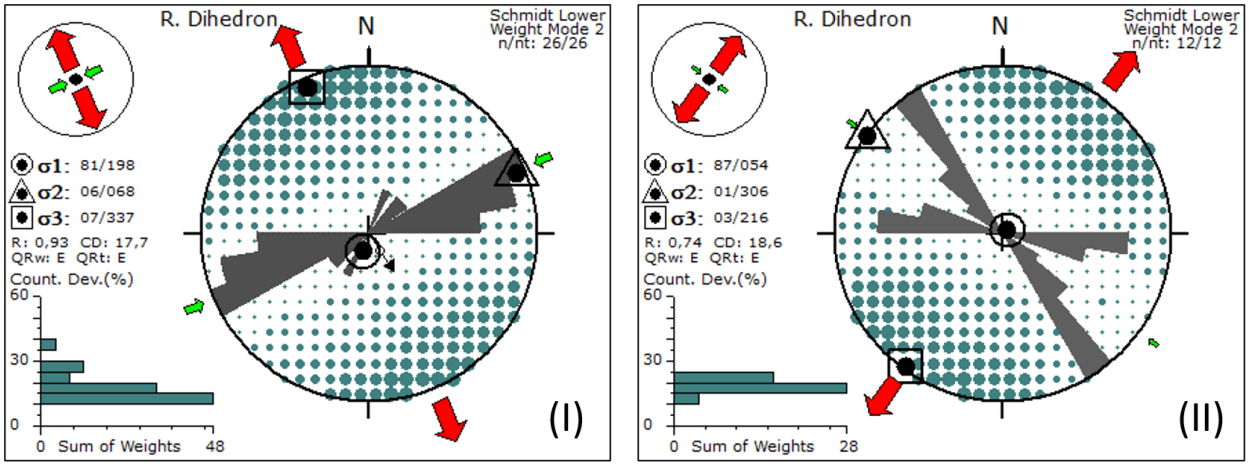

Figure 15. Stress tensor produced by ENE-WSW (I) and WNW-ESE to NW-SE (II) lamprophyre groups.

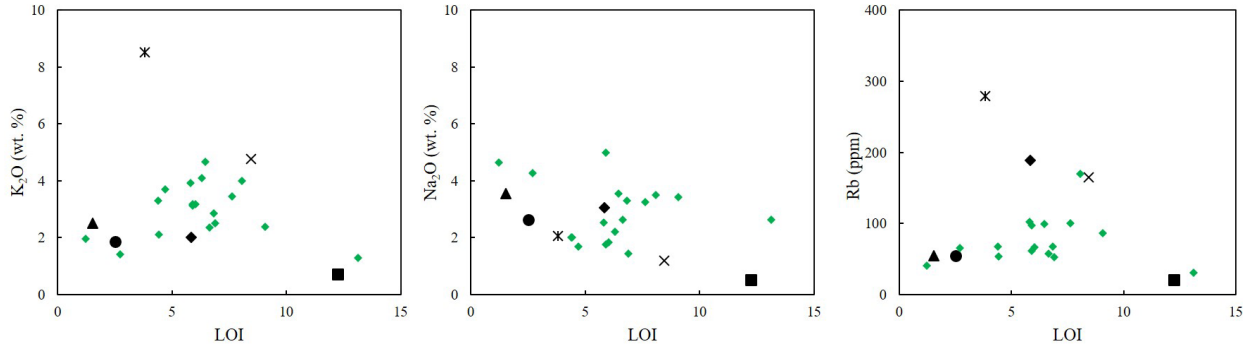

Figure 16. Variation diagrams between mobile elements and LOI (wt.%). Symbols as in Fig. 5.

(Melluso *et al.* 2017). Herein presented and compiled major and trace elements data from the Resende lamprophyre dykes show a continuous evolutional trend toward under-saturated evolved rocks and are in consonance with this statement. In addition, few recently discovered mafic alkaline rocks in the IAM, including mafic dykes (Rosa and Ruberti 2018), plot inside or near the Resende lamprophyres TAS range (Fig. 5). Furthermore, all Resende lamprophyre samples appear in the same field as or near the CFA lamprophyres (for most diagrams), confirming that this dyke swarm belongs to a regional mafic alkaline magmatism.

Mantle source characteristics

No mantle nodules were found in the new Resende lamprophyre dykes presented. However, spinel lherzolite nodules were found by Thompson *et al.* (1998) in a mica-rich lamprophyre at the same location of the MBN-65 lamprophyre dyke. According to these authors, some alkaline mafic dykes were generated by small degrees (1-8%) of partial melting of the "OIB-like anhydrous lherzolite source" beneath ca. 70 km (spinel-garnet transition zone). The La/Nb versus La/Ba plot (Fig. 17A) confirms a OIB affinity for the less evolved (MgO > 6 %) Resende lamprophyres (*e.g.* Guedes *et al.* 2005, Marins 2012, Brotzu *et al.* 2005). Orejana *et al.* (2008) state that a 100 times LREE enrichment coupled with a 10 times HREE enrichment over chondrite values imply the presence of residual garnet in a mantle source that has undergone low degrees of partial melting. However, trace element ratios do also indicate that the mantle sources may have been more enriched than OIB (Fig. 17B). Brotzu *et al.* (1997), Valente (1997), Gibson *et al.* (1999), Marins (2012) and Ferroni *et al.* (2018) agree with a previously enriched heterogeneous subcontinental lithospheric mantle source for the Resende lamprophyres and nearby areas. The Th/Yb versus Ta/Yb plot diagram does also confirm a within-plate mantle source for the Resende lamprophyres and the predominance of fractional crystallization over crustal assimilation on its evolution (Fig. 17B).

It is possible that the petrogenesis of the Resende lamprophyres is related with the presence of residual carbonate and clinopyroxene as well as residual biotite-phlogopite and/or kaersutite in the mantle source, the latter also being suggested previously by Brotzu *et al.* (2005). The enrichment of phlogopite and amphibole, and K_2O high contents plus Rb troughs displayed by some of the least evolved samples combined with LILE enrichment confirms a biotite-phlogopite- and/or kaersutite-bearing mantle source for some of the Resende lamprophyres. Farther Southeast, a phlogopite-bearing carbonate-metasomatised peridotite is suggested as a main source for at least some of the evolved lamprophyres in the Serra do Mar alkaline Province (SMAP; Azzone *et al.* 2018).

Structural implications

Resende lamprophyre dyke swarm emplacement

According to the structural analysis performed on this work, the Resende lamprophyre dyke swarm emplacement was controlled by an NNW-distension on a directional extensional regime, which resulted on numerous ENE-oriented dykes. Several dykes were also emplaced on previous WNW to NW joint sets, following basement parallel fractures (crustal discontinuities). Recent results concerning the Resende basin evolution, mention the NE-SW preferential direction to Upper Cretaceous lamprophyre dykes near the basin, with a NW-SE secondary set (Negrão *et al.* 2020). However, some authors point to a WNW-trend as the preferential direction to alkaline mafic dyke emplacement on this region in a perpendicular distention (NNE), related to the Cabo Frio Alignment (*e.g.* Ferroni *et al.* 2018). Herein and previous regional basement fracture data (*e.g.* Guedes *et al.* 2005, Ferroni *et al.* 2018) confirm WNW- to NW-oriented main directions that encompass more than forty joints affecting the local basement. This fact suggests a preferential basement discontinuity parallel to CFA, on the WNW direction, that acted as a previous pathway to magmatic flow, also suggested by Ferroni *et al.* (2018) among others (*e.g.* Almeida 1991, Riccomini *et al.* 2005). Field relationships confirm the occurrence of WNW- and NW-trending fractures prior to the lamprophyre dyke emplacement, which

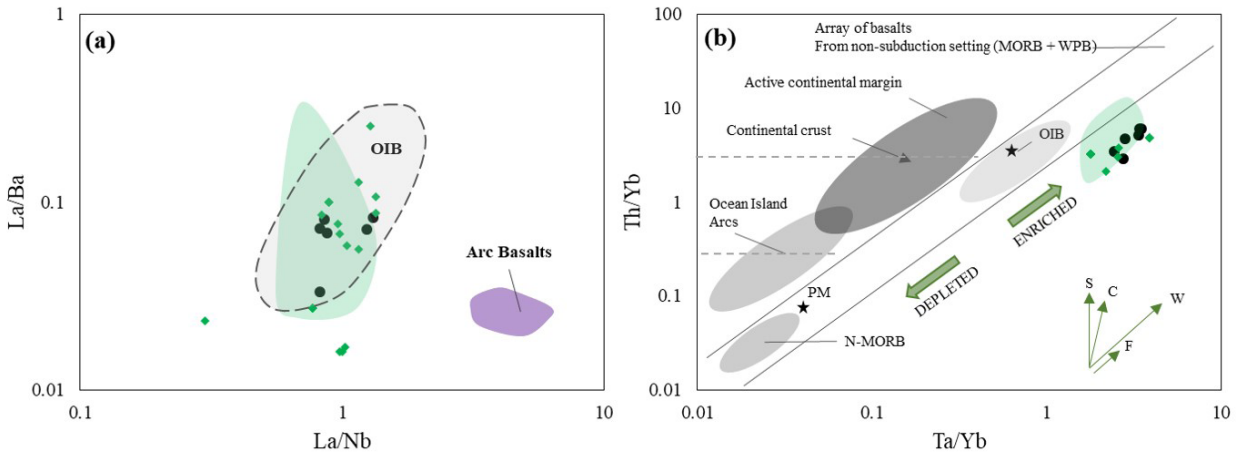

Figure 17. Variation diagrams using immobile trace element ratios. Symbols for the Resende lamprophyres as in Fig. 5. (A) La/Nb versus La/Ba plot (OIB field after Fitton *et al.* 1991). (B) Ta/Yb versus Th/Yb plot (after Menzies and Kyle 1990). Green arrows: (s) subduction zone enrichment, (c) crustal contamination, (w) within-plate enrichment, (f) fractional crystallization. PM is primitive mantle.

validate a fracture-controlled intrusion for WNW and NW directions.

Despite this, as detailed in the Structural Results, there is evidence that most dykes have been controlled by an NNW extension, in addition to minor control by previous structures on the same direction. The proof of this phenomenon is the the predominance of straight ENE-trending dykes with no offsets, representing type-I fractures, developed exclusively by an extension perpendicular to the dyke walls. It is relevant to state that those dykes were classified as good paleoindicators according to valid criteria (*e.g.* Delaney *et al.* 1986, Magee *et al.* 2019). Lamprophyre bodies in normal ENE-WSW fault planes on a possible syn-emplacement dynamic, plus the sub-horizontal average NNW-dilation direction observed allows the positioning of the main local extensional tensor (σ_3) at NNW (339/20), coinciding with the NNW-SSE direction and the value of 337/07 for the σ_3 tensor obtained from the inversion of the main dataset from the principal ENE-WSW set. Figure 18 illustrates the possible emplacement settings and its relationship with basement structural framework and stress axis position during the Resende lamprophyre dykes intrusion. Other works that used this method (Bussel 1989) obtained similar results, where the directions of the dyke dilations that intrude previous fractures indicate a different extension from what was expected from the main segments, that is, the real extension is not perpendicular to the walls of these bodies (Martínez-Poza *et al.* 2014, Stephens *et al.* 2017). These offset dykes also comprise secondary set direction, which means that the main set (ENE-WSW) fit to extension found by local and regional dilation. These authors used the criteria of Delaney *et al.* (1986) and the concepts of the Bussel's Method (Bussel 1989) to determine the paleoforces from the direction of the main bodies and the dilation direction.

In addition, the normal fault with a coeval lamprophyre dyke is exactly at the strike of a ten kilometers regional fault (Riccomini 1989, Guedes *et al.* 2005, Zalán and Oliveira 2005, Negrão *et al.* 2020). This relationship indicates that some of these lineaments have likely intrinsic origin during this magmatism and represent main faults that bound ENE-elongated basins, such as the Resende basin. In addition, the ENE-trending dykes not only use the anisotropy of the most deformed basement rocks (*e.g.* Ferroni *et al.* 2018), but also intrude in more isotropic lithotypes without previous fractures nor foliation. Thus, it is feasible that the regional paleotensors during this magmatism were positioned in this way, or not far from this arrangement:

- σ_1) sub-vertical in the 198/81 direction;
- σ_2) sub-horizontal in the 69/06 direction;
- σ_3) sub-horizontal around the 339/20 and 337/07 direction.

As seen earlier, these tensors were obtained using the Bussel's Method and the WinTensor software (Delvaux and Sperner 2003). Savastano *et al.* (2017) obtained satisfactory results from this method in kinematic and deformational analyzes on dykes, fractures and faults associated to the South Atlantic opening at the Cabo Frio (RJ) region. Similarly, other analyzes have generated accurate structural and deformational models in comparison to ENE-trending normal faults and dykes at Trindade Island (Barão *et al.* 2020). WinTensor was also used recently to determine the direction of the paleotensors during the multi-stage Resende basin evolution (Negrão *et al.* 2020).

In the regime obtained for the current work, the inferred maximum stress axis (σ_1) is sub-vertical, indicating a tectonic

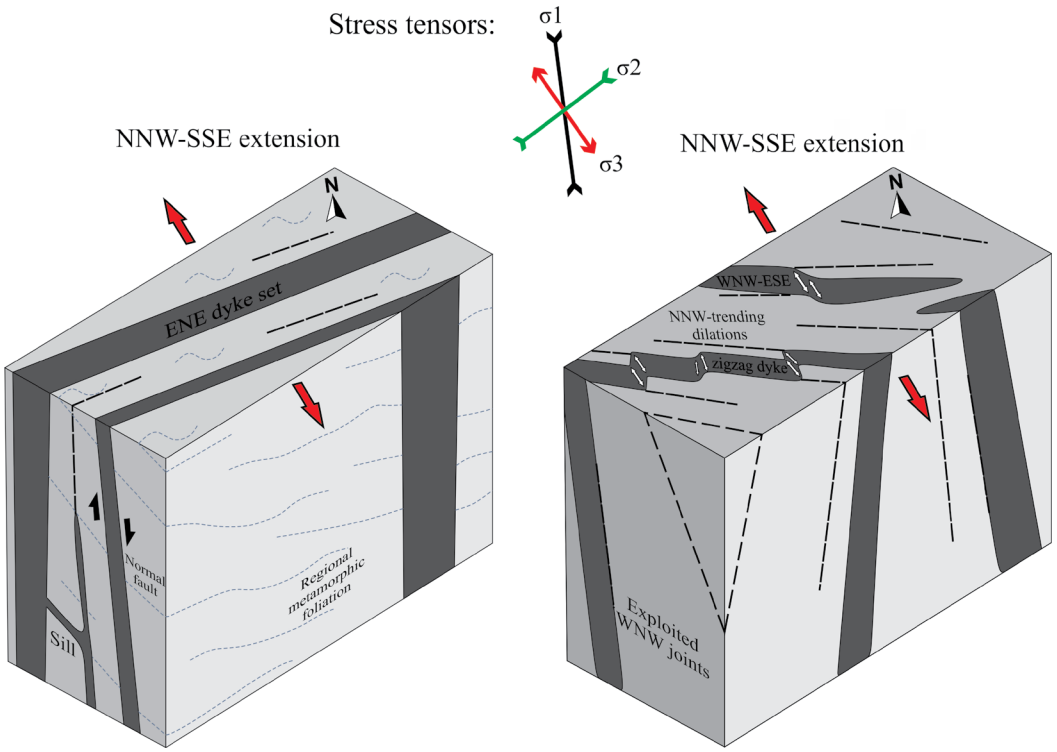

Figure 18. 3D sketches illustrating both ENE-trending straight predominant set and zigzag WNW-oriented secondary set emplaced at previous joints. All these structural features point to an NNW-SSE extension in pure extensional regime.

extension during the Resende lamprophyre dyke swarm emplacement. ENE-oriented compressive σ_2 would have a magnitude relatively greater than σ_3 ($R = \sigma_2-\sigma_3/\ \sigma_1-\sigma_2 = 0.93$), which possibly would impose stresses in the contraction sense to previous WNW fractures. However, the oblique positioning between σ_2 (ENE-WSW) and the WNW-ESE dykes, would possibly reduce this effect. In addition, volatile magmas such as the lamprophyres, have a high fluid pressure, capable of emplacing in narrow fractures in a rapid intrusion (Currie and Ferguson 1970). The presence of chilled margins and dendritic opaques also point to a rapid cooling in a dynamic intrusion (Vernon 2018).

Regional tectono-magmatism

Throughout this work, the cross-cut relationship between tholeiitic and lamprophyre dykes was not observed, but this kind of interaction was found previously. The presence of this feature on the north Resende basin indicates that the first one is older than the last, since the lamprophyre body intruded not only the basement, but also a diabase dyke, as observed by Riccomini (1989). In addition to this local relationship, tholeiitic dykes nearby or inserted on the study area have an established age range between 132 to 147 Ma, whereas an 82.6 lamprophyre dyke confirms that mafic alkaline magmatism is younger than the tholeiitic (Guedes *et al.* 2005). Two other ages from the Resende lamprophyre dykes also corroborate this geochronological statement and further outline its minimum interval, between 84.0 and 72.0 Ma (Riccomini *et al.* 1991, Ramos *et al.* 2008). Additionally, an apatite fission track age (FTA) was found on the detritic apatite from the Resende basin sediments and it is consistent to this interval (84.3 ± 6 Ma; Genaro 2008). An alkaline lamprophyre from SMAP presents a $^{40}Ar/^{39}Ar$ age of 85.7 ± 0.7 Ma (Azzone *et al.* 2018) that may suggest a relationship between these two magmatic expressions and other lamprophiric rocks from SE Brazil that present a similar age range (Thompson *et al.* 1998, Coutinho 2008, Azzone *et al.* 2009).

ASTER analytical results on the region (Souza, 2008) point to a majority of longer NE lineaments than shorter NNW and NW secondary directions. The main regional NE- to ENE-trending lineament ages at Rio de Janeiro range from 95 to 65 Ma (Tello *et al.* 2003, Hackspacher *et al.* 2004, Genaro 2008). This interval fits satisfactorily with the 89 to 65 Ma range established to basement uplift, responsible for alkaline magmatism emplacement (Zalán and Oliveira 2005). We argue that the Resende lamprophyre dyke was emplaced on this context, during the Upper Cretaceous, as the first regional alkaline magmatism, preceding major felsic alkaline intrusions, such as IAM. We also reinforce the possibility of Resende lamprophyre dykes as a mafic precursor of nearby felsic alkaline stocks) based on aforementioned data and interpretation. The lack of felsic alkaline rocks crosscut by lamprophyre dyke supports this hypothesis as well as the geochemical modeling performed by Rosa (2017).

NNW-SSE distension was the main emplacement control for the Resende lamprophyre dyke swarm. Our paleotensor directions are concordant with most tectono-sedimentary models for that region at the Upper Cretaceous/Paleogene (*e.g.* Riccomini 1989, Riccomini *et al.* 2004, Zalán and Oliveira 2005, Negrão *et al.* 2020). Compiled Resende lamprophyre ages (84.0 to 72.0 Ma) fits on this interval. Additionally, nearby Upper Cretaceous dyke swarms, such as those extending from Santos to Rio, were emplaced in the crust under a NW-SE horizontal extension (Tomba 2012). Furthermore, some nearby NE-trending lamprophyre dykes from the Passa Quatro Massif were previously related to the Cenozoic basin's first tectonic phase (*e.g.* Chiessi 2004). As stated by Riccomini *et al.* (2004), an NNW-trending distension was the first tectonic stage of the Resende basin's development during the Paleogene, which generates parallel hemi-grabens through which thick sediments from eroded uplifted basement were deposited. Negrão *et al.* (2020), in a correlated interpretation, also points to a NW- to NNW-trending direction to this Paleogene distension as the oldest developmental event of the Resende basin during the Pre-Rift stage. It is possible that this NNW-oriented distention endured from the Upper Cretaceous to the Paleogene or during this time, interval pulses with extensions very close to the positioning of the tensors have occurred. The presence of phonolite and trachyte dykes in the area ranging from 69 to 59 Ma ($^{40}Ar/^{39}Ar$ and $^{40}K/^{40}Ar$ plagioclase and whole rock) and trending preferentially along the ENE-WSW direction parallel and along the main Resende basin normal faults (*e.g.* Guedes *et al.* 2005, Ramos *et al.* 2008) suggest that the emplacement of these bodies was likely controlled by a similar direction stress axis (σ_3 at NNW, perpendicular to ENE-trending alkaline felsic dyke walls).

Meanwhile, WNW-trending lamprophyre dykes were inserted on previous basement fractures as observed. This secondary dyke direction is parallel to regional fractures that affect only metamorphic basement terrains (*e.g.* Guedes *et al.* 2005, Ferroni *et al.* 2018) and possibly reflect the CMA direction (*e.g.* Almeida 1983, Riccomini *et al.* 2005). Regarding NW- to NNW-oriented minor subset, it is related to regional parallel lineaments on fracture zones that were reactivated over Cenozoic as accommodation zones (*e.g.* Riccomini 1989, Valeriano and Heilbron 1993, Riccomini *et al.* 2004, Guedes *et al.* 2005, Zalán and Oliveira 2005). There is evidence of NW-trending lamprophyre dyke overprinting the Volta Redonda Transfer Zone, which suggests a previous weakness zone in such direction (Negrão *et al.* 2020). Both NNE-SSW and WNW-ESE directions may represent previous crustal discontinuities that were exploited by alkaline magmatic flow along the crust (*e.g.* Ferroni *et al.* 2018), however the Upper Cretaceous NNW-SSE brittle extension appears to be the main control of the Resende lamprophyre dyke swarm emplacement.

CONCLUSION

The crystalline basement near the Resende basin and the IAM are crosscut by at least 60 lamprophyre dykes. All types of alkaline lamprophyres, *i.e.*, sannaite, camptonite and monchiquite, occur but the latter is predominant. Physical characteristics and mineralogy are similar to the previous descriptions of the lamprophyre dykes occurring near the study area. These mafic alkaline intrusions compose an Upper Cretaceous dyke swarm which precedes the main felsic alkaline stocks and dykes, as well as the Resende basin. The relatively

more evolved ultrapotassic lamprophyres were included in a wider range of sodic and potassic types in the Resende lamprophyre dyke swarm. Fractional crystallization is the main petrological process that affects the Resende lamprophyres' evolution, controlled by the early fractionation of clinopyroxene and possibly olivine, presenting most abundantly as phenocrysts in these rocks, crustal contamination being negligible despite the occurrence of xenoliths and xenocrysts. The lack of feldspar as a phenocryst and Eu/Eu* ratio (0.91 to 1.16) precludes feldspar as a fractionation phase. Liquid immiscibility, rapid cooling, and autometassomatism also may have also occurred as depicted due to the presence of carbonate ocelli, dendritic opaques and chilled margins, as well as pseudomorphosed olivines. Whole-rock chemistry and petrography support this hypothesis and CFA lamprophyres present similar evolution. Trace elements patterns as well as trace element ratios (*e.g.*, Th/Yb and Ta/Yb) are consistent with derivation from a within-plate, fertile mantle source for the Resende lamprophyres, although mixing source processes with enriched mantle sources cannot be totally discarded. In addition to the presence of residual carbonate in the source as previously suggested, we point to a biotite-phlogopite- and/or kaersutite-bearing mantle source due to the presence of phlogopite and amphibole as phenocrysts, K_2O high contents plus Rb troughs displayed by some of the least evolved samples, as well as the overall LILE enrichment.

As seen, the crystalline basement displays two very clear and well-described discontinuities in that region, an ENE-trending foliation dipping ~60° towards SSE and a set of joints oriented WNW-ESE. The principal ENE-trending set present straight subvertical non-offsetted dykes classified as good paleoindicators, and they point to an NNW-SSE extension. On the other hand, secondary WNW to NW-oriented sets present zigzag dykes emplaced along previous WNW to NW-trending joints and transfer zones, making their guides unreliable for inclusion in the structural model as well as confirming that these dykes were controlled by previous paths along the crust. Wintensor analysis and Bussel's Method application as well as field measurements (normal faults and slickenlines/slickensides) and hierarquical positions confirm an NNW-SSE extension.

Our structural model allows the positioning of the minimum paleostress axis in the NNW-SSE orientation, very close to the orientation of the extension responsible for the first stage Resende basin tectono-sedimentary evolution, in the Paleogene. As reviewed, the Resende lamprophyres are related to an Upper Cretaceous magmatism (minimum interval between 84.0 and 72.0 Ma) and its activity is coeval to the Resende basin basement uplift and ENE-trending lineaments in this area. Therefore, a pure extension regime with a sub-horizontal minimum stress axis ($\sigma 3$) positioned around 339/20 and 337/07 direction is likely the main structural control for the Resende lamprophyre dyke swarm emplacement.

ARTICLE INFORMATION

Manuscript ID: 20210043. Received on: 13 JUN 2021. Approved on: 06 DEC 2021.

How to cite this article: Macedo B.N., Peternel R., Santos A.C., Simas M.P. Resende lamprophyres: new petrological and structural interpretations for a regional Upper Cretaceous alkaline mafic dyke swarm. *Brazilian Journal of Geology*, 52(1):e20210043, 2022. https://doi.org/10.1590/2317-4889202120210043.

B.M.: conceptualization, methodology, fieldwork, rock sampling, structural, petrographic and geochemical analysis, map preparation, and writing; R.P.: conceptualization, fieldwork, rock sampling, structural and petrographic analysis analysis, funding acquisition, review, and editing; A.S.: petrographic and geochemical analysis, methodology, investigation, funding acquisition, review and editing; M.S: fieldwork and structural analysis.

Competing interests: The authors declare no competing interests.

REFERENCES

Almeida F.F.M. 1983. Relações tectônicas das rochas alcalinas mesozóicas da região meridional da Plataforma Sul-Americana. *Revista Brasileira de Geociências*, **13**(3):139-158.

Almeida F.F.M. 1991. O alinhamento magmático de Cabo Frio. *In*: Simpósio de Geologia, 2., 1991, São Paulo e Rio de Janeiro. *Atas*... SBG, p. 423-428.

Almeida M.E.A. 1996. *Geologia, petrografia e geoquímica do Leucogranito Capivara, Itamonte (MG)*. Ms Dissertation, Instituto de Geociências, Universidade Federal do Rio de Janeiro, Rio de Janeiro, 128 p.

Anderson E.M. 1951. *The dynamics of faulting and dyke formation with application to Britain*. Edinburgh: Oliver and Boyd, 206 p.

Angelier L. 1991. Inversion directc de recherche 4-D: comparaison physique et mathematique de deux methodes de determination des tenseurs des paleocontraintcs en tectonique de failles. *C.R. Acad. Sci. Paris*, **312**(e):1213-1218.

Angelier L. 1994. Fault slip analysis and paleostress reconstruction. *In*: Hancock P.L. (Ed.). *Continental Deformation*. Oxford: Pergamon, p. 101-120.

Alves F.R. 1997. *Contribuição ao conhecimento geológico e petrográfico das rochas alcalinas da Ilha dos Búzios, SP*. PhD Thesis, Instituto de Geociências, Universidade de São Paulo, São Paulo.

Alves F.R., Gomes C.B. 2001. Ilha dos Búzios, litoral norte do estado de São Paulo: aspectos geológicos e petrográficos. *Geologia USP. Série Científica*, **1**:101-114. https://doi.org/10.5327/S1519-874X2001000100007

Araújo A.L. 1995. *Geologia, geoquímica e petrologia das rochas alcalinas da Ilha do Cabo Frio e das áreas continentais adjacentes, Arraial do Cabo - RJ*. Ms Dissertation, Programa de Pós-Graduação em Geologia, Universidade Federal Fluminense, Rio de Janeiro, 114 p.

Azzone R.G. 2008. *Petrogênese do maciço alcalino máfico-ultramáfico Ponte Nova (SP-MG)*. PhD Thesis, Instituto de Geociências, Universidade de São Paulo, São Paulo.

Azzone R.G., Ruberti E., Lopes da Silva J.C., Gomes C.B., Rojas G.E.E., Hollanda M.H.B.M., Tassinari C.C.G. 2018. Upper Cretaceous weakly to strongly silica-undersaturated alkaline dyke series of the Mantiqueira Range, Serra do Mar alkaline province: Crustal assimilation processes and mantle source signatures. *Brazilian Journal of Geology*, **48**(2):373-390. https://doi.org/10.1590/2317-4889201820170089

Azzone R.G., Ruberti E., Rojas G.E.E., Gomes C.B. 2009. Geologia e Geocronologia do Maciço Alcalino Máfico-Ultramáfico Ponte Nova (SP-MG). *Geologia USP. Série Científica*, **9**(2):23-46. https://doi.org/10.5327/Z1519-874x2009000200002

Barão L.M., Trzaskos B., Angulo R.J., Souza M.C. 2020. Deformation and structural evolution of mantle peridotites during exhumation on transform faults: A forced transition from ductile to brittle regime. *Journal of Structural Geology*, **133**:103981. https://doi.org/10.1016/j.jsg.2020.103981

Bennio L., Brotzu P., Gomes C.B., D'Antonio M., Lustrino M., Melluso L., Morbidelli L., Ruberti E. 2002. Petrological, geochemical and Sr- Nd isotopic features of alkaline rocks from the Arraial do Cabo Frio peninsula (southeastern Brazil). *Periodico di Mineralogia*, **71**(2):137-158.

Brotzu P., Beccaluva L., Conte A., Fonseca M., Garbarino C., Gomes C.B., Leong R., Macciotta G., Mansur R.L., Melluso L., Morbidelli L., Ruberti E., Sigolo J.B., Traversa G., Valença J.G. 1989. Petrological and geochemical studies of alkaline rocks from continental Brazil. The syenitic intrusion of Morro Redondo, RJ. *Geochimica Brasiliensis*, **3**(1):63-80.

Brotzu P., Gomes C.B., Melluso L., Morbidelli L., Morra V., Ruberti E. 1997. Petrogenesis of coexisting SiO2-undersaturated to SiO2-oversaturated felsic igneous rocks: the alkaline complex of Itatiaia, southeastern Brazil. *Lithos*, **40**(2-4):133-156. https://doi.org/10.1016/S0024-4937(97)00007-8

Brotzu P., Melluso L., D'Amelio F., Lustrino M. 2005. Potassic dykes and intrusions of the Serra do Mar Igneous Province (SE Brazil). *In*: Comin-Chiaramonti P., Gomes C.B. (Eds.). *Mesozoic to Cenozoic alkaline magmatism in the Brazilian Platform*. São Paulo: Edusp, p. 443-472.

Bussel M.A. 1989. A simple method for the determination of the dilation direction of intrusive sheets. *Journal of Structural Geology*, **11**(6):679-687. https://doi.org/10.1016/0191-8141(89)90004-7

Chiessi C.M. 2004. *Tectônica cenozoica no maciço alcalino de Passa Quatro (SP-MG-RJ)*. Ms Dissertation – Instituto de Geociências, Universidade de São Paulo, São Paulo.

Comin-Chiaramonti P., Cundari A., Piccirillo E.M., Gomes C.B., Castorina F., Censi P., De Min A., Marzoli A., Speziale S., Velázquez V.F. 1997. Potassic and sodic igneous rocks from Eastern Paraguay: Their origin from the lithospheric mantle and genetic relationships with the associated Paraná flood tholeiites. *Journal of Petrology*, **38**(4):495-528. https://doi.org/10.1093/petroj/38.4.495

Comin-Chiaramonti P., Gomes C.B. 2005. *Mesozoic to Cenozoic alkaline magmatism in the Brazilian Platform*. São Paulo: Edusp/Fapesp, 752 p.

Cooper A.F. 1979. Petrology of Ocellar Lamprophyres from Western Otago, New Zealand. *Journal of Petrology*, **20**(1):139-163. https://doi.org/10.1093/petrology/20.1.139

Coutinho J.M.V. 2008. Dyke Swarms of the Paraná Triple Junction, Southern Brazil. *Geologia USP. Série Científica*, **8**(2):29-52. https://doi.org/10.5327/z1519-874x2008000200003

Currie K.L., Ferguson J. 1970. The mechanism of intrusion of lamprophyredykes indicated by "offsetting" of dykes. *Tectonophysic*, **9**(6):525-535. https://doi.org/10.1016/0040-1951(70)90003-X

Delaney P.T., Pollard D.D., Ziony J.I., McKee E.H. 1986. Field relations between dykes and joints emplacement processes and paleostress analysis. *Journal of Geophysical Research*, **91**(B5):4920-4938. https://doi.org/10.1029/JB091iB05p04920

Delvaux D., Sperner B. 2003. New aspects of tectonic stress inversion with reference to the TENSOR program. *In*: Nieuwland D.A. (Ed.), *New insights into structural interpretation and modelling*. London, Geological Society, Special Publications, **212**:75-100.

Enrich G.E.R., Azzone R.G., Ruberti E., Gomes C.B., Comin-Chiaramonti P. 2005. Itatiaia, Passa Quatro and São Sebastião Island, the major alkaline syenitic complexes from the Serra do Mar region. *In*: Comin-Chiaramonti P., Gomes C.B. (Eds.). *Mesozoic to Cenozoic alkaline magmatism in the Brazilian Platform*. São Paulo: Edusp, p. 419-441.

Ferrari A.L. 2001. *Evolução tectônica do Gráben da Guanabara*. PhD thesis, Universidade de São Paulo, Instituto de Geociências, São Paulo.

Ferroni F.R., Mello C.L., Destro N. 2018. Tectonic control on the Cabo Frio anorogenic magmatic lineament, Southeastern Brazil. *Journal of South American Earth Sciences*, **83**:37-54. https://doi.org/10.1016/j.jsames.2017.11.001

Fitton J.G., James D., Leeman W.P. 1991. Basic magmatism associated with Late Cenozoic extension in the western United States: compositional variations in space and time. *Journal of Geophysical Research*, **96**(B8):13693-13711. https://doi.org/10.1029/91JB00372

Fitton J.G., Upton B.G.J. 1987. *Alkaline igneous rocks*. Geological Society Special Publication, 30, 568 p.

Foley S.F., Venturelli G., Green D.H., Toscani L. 1987. The ultrapotassic rocks; characteristics, classification, and constraints for petrogenetic models. *Earth-Science Reviews*, **24**(2):81-134. https://doi.org/10.1016/0012-8252(87)90001-8

Fonseca M.A., Pinto C.P., Silva M.A. 2014. *Mapa Geológico do Estado de Minas Gerais, escala 1:1.000.000*. Secretaria de Geologia, Mineração e Transformação Mineral, Serviço Geológico do Brasil.

Fossen H. 2010. *Structural geology*. Cambridge, Cambridge University Press, 463 p.

Garda G.M. 1995. *Os diques básicos e ultrabásicos da região costeira entre as cidades de São Sebastião e Ubatuba, Estado de São Paulo*. PhD thesis, Universidade de São Paulo, São Paulo. https://doi.org/10.11606/T.44.1995.tde-20032013-160227

Garda G.M., Schorscher J.H.D., Esperança S., Carlson R.W. 1995. The petrology and geochemistry of coastal dykes from São Paulo State, Brazil: Implication for variable litospheric contributions to alkaline magmas from the Western margins of the South Atlantic. *Anais da Academia Brasileira de Ciências*, **67**(2):191-216.

Genaro D.T. 2008. *Contribuição ao conhecimento de processos atuantes no rifteamento continental, por traços de fissão em zircões e apatitas, aplicados no rift continental do Sudeste do Brasil, bacias de Taubaté, Resende, Volta Redonda e Circunvizinhanças*. Ms Dissertation, Instituto de Geociências e Ciências Exatas, Universidade Estatual Paulista "Júlio de Mesquita Filho, Presidente Prudente, 131 p.

Gibson S.A., Thompson R.N., Leonardos O.H., Dickin A.P., Mitchell J.G. 1995. The Late Cretaceous impact of the Trindade mantle plume: Evidence from large-volume, mafic potassic magmatism in SE Brazil. *Journal of Petrology*, **36**(1):189-229. https://doi.org/10.1093/petrology/36.1.189

Gibson S.A., Thompson R.N., Leonardos O.H., Dickin A.P., Mitchell J.G. 1999. The limited extent of plume-lithosphere interactions during continental flood-basalt genesis: Geochemical evidence from Cretaceous magmatism in southern Brazil. *Contributions to Mineralogy and Petrology*, **137**(1-2):147-169. https://doi.org/10.1007/s004100050588

Gomes C.B., Comin-Chiaramonti P. 2005. An introduction to the alkaline and alkaline-carbonatitic magmatism in and around the Paraná-Basin. *In*: Comin-Chiaramonti P., Gomes C.B. (Eds.). *Mesozoic to Cenozoic alkaline magmatism in the Brazilian Platform*. São Paulo: Edusp/Fapesp, p. 21-30.

Guedes E., Heilbron M., Vasconcelos P.M., Valeriano C.M., Almeida J.C.H., Teixeira W., Thomaz Filho A. 2005. K/Ar and 40Ar/39Ar ages of dykes emplaced in the on-shore basement of the Santos Basin, Resende Area, SE Brazil: implications for the South Atlantic opening and Terciary reactivation. *Journal of South America Earth Sciences*, **18**(3-4):371-382. https://doi.org/10.1016/j.jsames.2004.11.008

Hackspacher P.C., Ribeiro L.F.B., Hadler Neto J.C., Tello S.C.A., Guedes S. 2004. Oligocen – Miocen heating of the South American Platform in Southeastern Brazil: Constraints from apatite fission track studies. *In*: International Geological Congress, Florence, 32., 2004. *Annals…*

Hauser M., Matteini M., Omarini R.H., Pimentel M.M. 2010. Constraints on metasomatized mantle under Central South America: evidence from Jurassic alkaline lamprophyre dykes from the Eastern Cordillera, NM Argentina. *Mineralogy and Petrology*, **100**(3-4):153-184. https://doi.org/10.1007/s00710-010-0127-5

Heilbron M., Eirado L.G., Almeida J. 2016. *Mapa geológico e de recursos minerais do estado do Rio de Janeiro, escala 1:400.000*. Belo Horizonte: Programa Geologia do Brasil (PGB), Mapas Geológicos Estaduais, Serviço Geológico do Brasil, Superintendência Regional de Belo Horizonte.

Heilbron M., Mohriak W.V., Valeriano C.M., Milani E.J., Almeida J., Tupinambá M. 2000. From collision to extension: the roots of the southeastern continental margin of Brazil. *In*: Talwani M., Mohriak W.U. (Eds.). *Atlantic rifts and continental margins*. Washington, D.C.: American Geophysical Union, Geophysical Monograph Series, **115**:1-34.

Heilbron M., Pedrosa-Soares A.C., Campos Neto M.C., Silva L.C., Trouw R.A.J., Janasi V.A. 2004. Província Mantiqueira. *In*: Mantesso-Neto V., Bartorelli A., Carneiro, C.D.R., Brito-Neves B.B. (Eds.). *Geologia do continente sul-americano:* evolução da obra de Fernando Flávio Marques de Almeida. São Paulo: Beca, p. 203-235.

Herz N. 1977. Timing of spreading in the South Atlantic: Information from Brazilian alkalic rocks. *Geological Society of America Bulletin*, **88**(1):101-112. https://doi.org/10.1130/0016-7606(1977)88%3C101:TOSITS%3E2.0.CO;2

Jiang Y.H., Jiang S.Y., Ling H.F., Ni P. 2010. Petrogenesis and tectonic implications of Late Jurassic shoshonitic lamprophyre dykes from the Liaodong Peninsula, NE China. *Mineralogy and Petrology*, **100**:127-151. https://doi.org/10.1007/s00710-010-0124-8

Le Bas M.J., Le Maitre R.W., Streckeisen A., Zanettin B. 1986. A Chemical Classification of Volcanic Rocks Based on the Total Alkali-Silica Diagram. *Journal of Petrology*, **27**(3):745-750. https://doi.org/10.1093/petrology/27.3.745

Le Bas M.J., Streckeisen A.L. 1991. The IUGS systematics of igneous rocks. *Journal of the Geological Society*, **148**(5):825-833. https://doi.org/10.1144/gsjgs.148.5.0825

Le Maitre R.W. 2002. *Igneous rocks*. A classification of igneous rocks and glossary of terms. 2ª ed. New York: Cambridge University Press.

Magee C., Muirhead J., Schofield N., Walker R.J., Galland O., Holford S., Spacapan J., Jackson C.A.L., McCarthy W. 2019. Structural signatures of igneous sheet intrusion propagation. *Journal of Structural Geology*, **125**:148-154. https://doi.org/10.1016/j.jsg.2018.07.010

Marins G.M. 2012. *Estudo do magmatismo máfico de complexos alcalinos do sudeste do Brasil*. Ms Dissertation, Universidade do Estado do Rio de Janeiro, Rio de Janeiro.

Martínez-Poza A.I., Druguet E., Castaño L.M., Carreras J. 2014. Dyke intrusion into a pre-existing joint network: the Aiguablava lamprophyre dyke swarm (Catalan coastal ranges). *Tectonophysics*, **630**:75-90. https://doi.org/10.1016/j.tecto.2014.05.015

McDonough W.F., Sun S. 1995. The composition of the Earth. *Chemical Geology*, **120**(3-4):223-253. https://doi.org/10.1016/0009-2541(94)00140-4

Melluso L., Guarino V., Lustrino M., Morra V., Gennaro R. 2017. The REE- and HFSE-bearing phases in the Itatiaia alkaline complex (Brazil), and geochemical evolution of feldspar-rich felsic melts. *Mineralogical Magazine*, **81**(2):217-250. https://doi.org/10.1180/minmag.2016.080.122

Menzies M.A., Kyle P. 1990. Continental volcanism: a crust-mantle probe. *In*: Menzies M.A. (Ed.), *The Continental Mantle*. Oxford: Clarendon Press, p. 157-177.

Mohriak W.U. Recursos energéticos associados à ativação tectônica mesozóica-cenozóica da América do Sul. *In*: Mantesso-Neto V., Bartorelli A., Carneiro C.D.R., Brito-Neves B.B. (Eds.). *Geologia do continente Sul-Americano:* evolução da obra de Fernando Flávio Marques de Almeida. São Paulo: Beca, 2004. p. 293-318.

Morbidelli L., Gomes C.B., Beccaluva L., Brotzu P., Conte A.M., Ruberti E., Traversa G. 1995. Mineralogical, petrological and geochemical aspects of alkaline and alkaline-carbonatite associations from Brazil. *Earth-Sciences Review*, **39**(3-4):135-168. https://doi.org/10.1016/0012-8252(95)00031-3

Mota C.E.M. 2012. *Petrogênese e geocronologia das intrusões alcalinas de Morro Redondo, Mendanha e Morro São João: caracterização do magmatismo alcalino no Estado do Rio de Janeiro e implicações geodinâmicas*. PhD Thesis, Faculdade de Geologia, Universidade do Estado do Rio de Janeiro, Rio de Janeiro, 204 p.

Motoki A., Motoki K., Santos A.C., Nogueira C.C., Santos W.H., Geraldes M.C., Sichel S., Vargas T. 2018. Geology, petrology and magmatic evolution of the felsic alkaline rocks of the Vitória Island, São Paulo State, Brazil. *Anuário do Instituto de Geociências*, **41**(3):125-136. https://doi.org/10.11137/2018_3_125_136

Motoki A., Sichel, S.E., Savi, D.C., Aires, J.R. 2008. Intrusion mechanism of tabular intrusive bodies of subhorizontal discordant emplacement of the Cabo Frio Island and the neighbour areas, State of Rio de Janeiro, Brazil. *Geociências*, **27**(2):207-218.

Motoki A., Sichel S.E., Soares R., Aires J.R., Netto A.M., Lobato M. 2007. Genetic reconsideration of the Nova Iguaçu Volcano model, State of Rio de Janeiro, Brazil: eruptive origin or subvolcanic intrusion? *Revista Escola de Minas*, **60**(4):583-592. https://doi.org/10.1590/S0370-44672007000400003

Motoki A., Sichel S.E., Vargas T., Aires J.R., Iwanuch W., Mello S.L.M., Motoki K.F., Silva S., Balmant A. 2010. Geochemical evolution of the felsic alkaline rocks of Tanguá, Rio Bonito, and Itaúna intrusive bodies, State of Rio de Janeiro, Brazil. *Geociências*, **29**(3):291-310.

Nakamura N. 1974. Determination of REE, Ba, Fe, Mg, Na and K in Carbonaceous and Ordinary Chondrites. *Geochimica et Cosmochimica Acta*, **38**(5):757-775. https://doi.org/10.1016/0016-7037(74)90149-5

Nédli Z., M. Tóth T. 2007. Origin and geotectonic significance of Upper Cretaceous lamprophyres from the Villány Mts (S Hungary). *Mineralogy and Petrology*, **90**(1):73-107. https://doi.org/10.1007/s00710-006-0168-y

Negrão A.P., Mello C.L., Ramos R.R.C., Sanson M.S.R., Louro V.H.A., Bauli P.G. 2020. Tectonosedimentary evolution of the Resende and Volta Redonda basins (Cenozoic, Central Segment of the Continental Rift of Southeastern Brazil). *Journal of South American Earth Sciences*, **104**:102789. https://doi.org/10.1016/j.jsames.2020.102789

Negrão A.P., Ramos R.R.C., Mello C.L., Sanson M.D.S.R. 2015. Mapa geológico do cenozoico da região da bacia de Volta Redonda (RJ, segmento central do Rifte Continental do Sudeste do Brasil): identificação de novos grabens e ocorrências descontínuas, e caracterização de estágios tectonossedimentares. *Brazilian Journal of Geology*, **45**(2):273-291. https://doi.org/10.1590/23174889201500020007

Ngounouno I., Déruelle B., Demaiffe D., Montigny R. 2003. Les monchiquites de Tchircotché, vallée de la haute Bénoué (Nord du Cameroun). *Comptes Rendus Geoscience*, **335**(3):289-296. https://doi.org/10.1016/S1631-0713(03)00047-6

Orejana D., Villaseca C., Billström K., Paterson B.A. 2008. Petrogenesis of Permian alkaline lamprophyres and diabases from the Spanish Central System and their geodynamic context within Western Europe. *Contributions to Mineralogy and Petrology*, **156**(4):477-500.

Pandey A., Chalapathi Rao N.V., Chakrabarti R., Pandit D., Pankaj P., Kumar A., Sahoo S. 2017. Petrogenesis of a Mesoproterozoic shoshonitic lamprophyre dyke from the Wajrakarur kimberlite field, eastern Dharwar craton, southern India: Geochemical and Sr-Nd isotopic evidence for a modified sub-continental lithospheric mantle source. *Lithos*, **292-293**:218-233. https://doi.org/10.1016/j.lithos.2017.09.001

Penalva F. 1967. Geologia e tectônica da região do Itatiaia (Sudeste do Brasil). *Boletim da Faculdade de Filosofia Ciências e Letras, Universidade de São Paulo. Geologia*, **302**(22):99. https://doi.org/10.11606/issn.2526-3862.bffcluspgeologia.1967.121904

Peternel R., Trouw R.A.J., Schmitt R.S. 2005. Interferência entre duas faixas móveis neoproterozóicas: o caso das Faixas Brasília e Ribeira no Sudeste do Brasil. *Revista Brasileira de Geociências*, **35**(3):297-310.

Phani P.R.C., Raju V.V.N., Srinivas M. 2018. Petrological and geochemical characteristics of a shoshonitic lamprophyre, Sivarampet, Wajrakarur Kimberlite Field, Southern India. *Journal of Applied Geology and Geophysics*, **6**(2):55-69. https://doi.org/10.9790/0990-0602015569

Pollard D.D. 1973. Derivation and evaluation of a mechanical model for sheet intrusions. *Tectonophysics*, **19**(3):233-269. https://doi.org/10.1016/0040-1951(73)90021-8

Pouclet A., El-Hadi H., Bardintzeff J.M, Benharref M., Fekkak A. 2017. Devonian to Early Carboniferous magmatic alkaline activity in the Tafilalt Province, Eastearn Morocco: An Eovariscan episode in the Gondwana margin, north of the West African Craton. *Journal of African Earth Sciences*, **129**:814-841. https://doi.org/10.1016/j.jafrearsci.2017.01.030

Raeisi D., Gholoizade K., Nayebi N., Babazadeh S., Nejadhadad M. 2019. Geochemistry and mineral composition of lamprophyre dykes, central Iran: implications for petrogenesis and mantle evolution. *Journal of Earth System Science*, **128**:74. https://doi.org/10.1007/s12040-019-1110-0

Ramos R.R.C., Avila C.A., Vasconselos P.M.P., Thiede D., Vasques F.S.G., Rocha F.M. 2008. Magmatismo Meso-cenozoico na região das Bacias de Resende e de Volta Redonda. *In*: Congresso Brasileiro de Geologia, 44., 2008. *Anais*... **35**:559.

Ribeiro Filho E. 1967. Geologia e petrologia dos maciços alcalinos do Itatiaia e Passa-Quatro. *Geologia*, (22):1-91. https://doi.org/10.11606/issn.2526-3862.bffcluspgeologia.1967.121901

Riccomini C. 1989. *O Rift continental do sudeste do Brasil*. PhD Thesis, Universidade de São Paulo, São Paulo, 256 p.

Riccomini C., Melo M.S., Coutinho J.M.V. 1991. Late cretaceous-early tertiary ultrabasic magmatism in the western part of the state of Rio de Janeiro, Brazil. *Boletim IG-USP, Publicação Especial*, (10):77-84. https://doi.org/10.11606/issn.2317-8078.v0i10p77-84

Riccomini C., Sant'anna L.G., Ferrari A.L. 2004. Evolução geológica do Rift Continental do Sudeste do Brasil. *In*: Mantesso-Neto V., Bartorelli A., Dal Ré Carneiro C., Brito Neves B. B. (Eds.). *Geologia do continente sul-americano – evolução da obra de Fernando Flávio Marques de Almeida*. São Paulo: Beca, p. 350-383.

Riccomini C., Velázquez V.F., Gomes C.B. 2005. Tectonic controls of the Mesozoic and Cenozoic alkaline magmatism in central-southeastern Brazilian Platform. *In*: Comin-Chiaramonti P., Gomes C.B. (Eds.). *Mesozoic to Cenozoic alkaline magmatism in the Brazilian Platform*. São Paulo: Edusp, p. 31-56.

Rock N.M.S. 1991. *Lamprophyres*. Glasgow: Blackie and Sons, 285 p.

Rosa P.A.S. 2017. *Geologia e evolução petrogenética do maciço alcalino de Itatiaia, MG-RJ*. PhD thesis, Universidade de São Paulo, São Paulo.

Rosa P.A.S., Ruberti E. 2018. Nepheline syenites to syenites and granitic rocks from the Itatiaia alkaline massif, SE Brazil: new geological insights of a migratory ring complex *Brazilian Journal of Geology*, **48**(2):347-372. https://doi.org/10.1590/2317-4889201820170092

Sadowski G.R., Dias Neto C.M. 1981. O lineamento sismo-tectônico de Cabo Frio. *Revista Brasileira de Geociências*, **11**(4):209-212.

Santos A.C. 2013. *Petrografia, litogeoquímica e datação Ar-Ar dos Montes Submarinos e dos rochedos de Martin Vaz – Cadeia Vitória-Trindade*. Ms Dissertation, Faculdade de Geologia, Universidade do Estado do Rio de Janeiro, Rio de Janeiro, 115 p.

Santos A.C. 2016. *Petrology of Martin Vaz Island and VitoriaTrindade Ridge seamounts: Montague, Jaseur, Davis, Dogaressa and Columbia. Trace elements, 40Ar/39Ar dating and Sr and Nd isotope analysis related to the Trindade Plume evidences*. PhD thesis, Universidade do Estado do Rio de Janeiro, Rio de Janeiro, 218 p.

Savastano V.L.M., Schmitt R.S., Araújo M.N.C., Inocêncio L.C. 2017. Rift brittle deformation of SE-Brazilian continental margin: kinematic analysis of onshore structures relative to the transfer and accommodation zones of southern Campos Basin. *Journal of Structural Geology*, **94**:136-153. https://doi.org/10.1016/j.jsg.2016.11.012

Scarrow J.H., Molina J.F., Bea F., Montero P., Vaughan A.P.M. 2011. Lamprophyre dykes as tectonic markers of late orogenic transtension timing and kinematics: a case study from the Central Iberian Zone. *Tectonics*, **30**(4). https://doi.org/10.1029/2010TC002755

Schmitt R.S., Trouw R.A.J., Van Schmus W.R., Pimentel M.M. 2004. Late amalgamation in the central part of Western Gondwana: new geochronological data and the characterization of a Cambrian collision orogeny in the Ribeira Belt (SE Brazil). *Precambrian Research*, **133**(1-2):29-61. https://doi.org/10.1016/j.precamres.2004.03.010

Sichel S.E., Motoki A., Iwanuch W., Vargas T., Aires J.R., Melo D.P., Motoki K.F., Balmant A., Rodrigues J.G. 2012. Fractionation crystallization and continental crust assimilation by the felsic alkaline rock magmas of the State of Rio de Janeiro, Brazil. *Anuário do Instituto de Geociências*, **35**(2):84-104. https://doi.org/10.11137/2012_2_84_104

Soder C., Altherr R., Romer R.L. 2016. Mantle metasomatism at the edge of a retreating subduction zone: late neogene lamprophyres from the Island of Kos, Greece. *Journal of Petrology*, **57**(9):1705-1728. https://doi.org/10.1093/petrology/egw054

Sonoki I.K., Garda G.M. 1988. Idades K-Ar de rochas alcalinas do Brasil Meridional e Paraguai Oriental: compilação e adaptação às novas constantes de decaimento. *Boletim IG-USP. Série Científica*, **19**:63-85. https://doi.org/10.11606/issn.2316-8986.v19i0p63-85

Stemprok M., Seifert T., Holub F.V., Chlupáčová M., Dolejš D., Novák J.D., Pivec E., Lang M. 2008. Petrology and geochemistry of Variscan dykes from the Jáchymov (Joachimsthal) ore district, Czech Republic. *Journal of Geosciences*, **53**(1):65-104. https://doi.org/10.3190/jgeosci.020

Stephens T.L., Walker R.J., Healy D., Bubeck A., England R.W., McCaffrey K.J.W. 2017. Igneous sills record far-field and near-field stress interactions during volcano construction: Isle of Mull, Scotland. *Earth and Planetary Science Letters*, **478**:159-174. https://doi.org/10.1016/j.epsl.2017.09.003

Stoppa F., Rukhlov A.S., Bell K., Schiazza M., Vichi G. 2014. Lamprophyres of Italy: early Cretaceous alkaline lamprophyres of Southern Tuscany, Italy. *Lithos*, **188**:97-112. https://doi.org/10.1016/j.lithos.2013.10.010

Streckeisen A.L., Le Maitre R. 1979. A chemical approximation to the modal QAPF classification of the igneous rocks. *Abhandlungen, Neues Jahrbuch fur Mineralogie*, **136**:169-206.

Tappe S., Foley S.F., Jenner G.A., Kjarsgaard B.A. 2005. Integrating ultramafic lamprophyres into the IUGS classification of igneous rocks: rationale and implications. *Journal of Petrology*, **46**(9):1893-1900. https://doi.org/10.1093/petrology/egi039

Tello S.C.A., Hadler Neto J.C., Iunes P.J., Guedes O.S., Hackspacher P.C., Ribeiro L.F.B., Paulo S.R., Osorio A.M. 2003. Termocronology of the south american platform in the state of são Paulo, through apatite fission tracks. *In*: South American Symposium on Isotope Geology, 4., 2003, Salvador. *Book of short papers…* p. 124-127.

Thomaz Filho A., Rodrigues A.L. 1999. O alinhamento de rochas alcalinas Poços de Caldas-Cabo Frio (RJ) e sua continuidade na Cadeia Vitória-Trindade. *Revista Brasileira de Geociências*, **29**(2):189-194.

Thompson R.N., Gibson S.A., Mitchell J.G., Dickin A.P., Leonardos O.H., Brod J.A., Greenwood J.C. 1998. Migrating Cretaceous–Eocene Magmatism the Serra do Mar Alkaline Province, SE Brazil: Melts from the Deflected Trindade Mantle Plume? *Journal of Petrology*, **39**(8):1493-1526. https://doi.org/10.1093/petroj/39.8.1493

Tomba C.L.B. 2012. *Análise estrutural dos enxames de diques máficos eocretaceos do Sul-Sudeste do Brasil*. Ms Dissertation, Instituto de Geociências, Universidade de São Paulo, São Paulo, 133 p.

Trouw R.A., Peternel R., Ribeiro A., Heilbron M., Vinagre R., Duffles P., Trow C.C., Fontainha M., Kussama H.H. 2013. A new interpretation for the interference zone between the southern Brasília belt and the central Ribeira belt, SE Brazil. *Journal of South American Earth Sciences*, **48**:43-57. https://doi.org/10.1016/j.jsames.2013.07.012

Ubide T., Arranz E., Lago M., Galé C., Larrea P. 2012. The influence of crystal settling on the compositional zoning of a thin lamprophyre sill: a multi-method approach. *Lithos*, **132-133**:37-49. https://doi.org/10.1016/j.lithos.2011.11.012

Ulbrich H.H.G.J., Gomes C.B. 1981. Alkaline rocks from continental Brazil. *Earth-Science Reviews*, **17**(1-2):135-154. https://doi.org/10.1016/0012-8252(81)90009-X

Ulbrich H.H.G.J., Vlach S.R.F., Demaiffe D., Ulbrich M.N.C. 2005. Structure and origin of the Poços de Caldas Alkaline Massif, SE Brazil. *In*: Comin-Chiaramonti P., Gomes C.B. (Eds.). *Mesozoic to cenozoic alkaline magmatism in the Brazilian Plataform*. São Paulo: Edusp/Fapesp, p. 367-418.

Valença J., Reis A.P., Carvalho Filho C.A., Soares Filho J.R.S., Braun P.V.C.B. 1983. Geologia do complexo ígneo alcalino do Morro Redondo (Município de Resende, Estado do Rio de Janeiro). *Anais da Academia Brasileira de Ciências*, 55:135-136.

Valente S.C. 1997. *Geochemical and isotopic constraints on the petrogenesis of the Cretaceous dykes of Rio de Janeiro, Brazil*. PhD thesis, Queen's University of Belfast, Belfast.

Valente S.C., Duarte B.P., Heilbron M., Corval A., Valladares C., Almeida J.C.H., Guedes E. 2005. Provincialidade geoquímica do Enxame de diques da Serra do Mar e domínios tectônicos do Orógeno Ribeira: o Cretáceo como uma janela para o Proterozóico. *In*: Simpósio Nacional de Estudos Tectônicos, 10., e International Symposium on Tectonics, 7., 2005. *Boletim de Resumos...*, p. 283-285.

Valeriano C, Heilbron M. 1993. A Zona de Transtensão de Volta Redonda e sua importância na junção entre os Riftes do Vale do Paraíba e da Guanabara: dados Preliminares. *In*: Simpósio de Geologia do Sudeste, 3., 1993. *Anais...* p. 9-15.

Ventura M.C., Valente S.V. 2017. Petrogênese da Suíte alcalina fortemente insaturada em sílica dos diques do Pontal do Atalaia, Arraial do Cabo, RJ. *In*: Congresso Brasileiro de Geologia, 48., 2017. *Anais...* p. 547.

Vernon R. 2018. *A practical guide to rock microstructure*. 2. ed. Cambridge: Cambridge University Press, 1472 p. https://doi.org/10.1017/9781108654609

Whitney D.L., Evans B.W. 2010. Abbreviations for names of rock-forming minerals. *American Mineralogist*, 95(1):185-187. https://doi.org/10.2138/am.2010.3371

Woolley A.R., Bergman S.C., Edgar A.D., Le Bas M., Mitchell R.H., Rock N.M.S., Smith B.H.S. 1996. Classification of lamprophyres, lamproites, kimberlites, and kasilitic, melilitic, and leucitic rocks. *The Canadian Mineralogist*, **34**:175-186.

Zalán P.V., Oliveira J.A.B. 2005. Origem e evolução estrutural do Sistema de Rittes Cenozóicos do Sudeste do Brasil. *Boletim de Geociências da Petrobras*, **13**(2):269-300.

Zoback M.L. 1992. First- and second-order patterns of stress in the lithosphere the World Stress Map Project. *Journal of Geophysical Research*, **97**(B8):11703-11728. https://doi.org/10.1029/92JB00132